Tribology International 198 (2024) 109896

Contents lists available at ScienceDirect

Tribology International

journal homepage: www.elsevier.com/locate/triboint

Structure, superlubricity, applications, and chemical vapor deposition methods of graphene solid lubricants

Shuyu Fan [a], Yinong Chen [a], Jing Wu [a], Shu Xiao [a,*], Guohua Chen [a], Paul K. Chu [b,*]

[a] School of Mechanical & Automotive Engineering, South China University of Technology, Guangzhou 510641, China
[b] Department of Physics, Department of Materials Science and Engineering, and Department of Biomedical Engineering, City University of Hong Kong, Tat Chee Avenue, Kowloon, Hong Kong, China

ARTICLE INFO

Keywords:
Graphene solid lubricants
Superlubricity
Macroscale
Harsh working conditions

ABSTRACT

Friction-induced wear is a major cause of energy consumption and equipment failure and graphene as a novel solid lubricant has become a hot topic in tribological engineering. Micro/nanoscale and macroscale superlubricity has been observed from graphene-based solid lubricants and the ability to mass produce high-quality graphene by chemical vapor deposition (CVD) is attractive, especially for applications requiring operation under harsh working conditions. This comprehensive review discusses the relationship between the structure and friction properties of solid graphene lubricants, mechanisms of macroscale superlubricity, applications pertaining to harsh working conditions, strategies to prolong macroscale superlubricity, as well as challenges in order to provide guidance for future research and development of graphene-based solid lubricants.

1. Introduction

Climate change poses significant global risks, making the development of green and low-carbon energy systems key to achieving carbon neutrality [1]. Mechanical components used in aviation, aerospace, marine, and automotive application fields, such as bearings, gears, and valves, are frequently subjected to complex chemomechanical interactions (Fig. 1a) [2–7]. These components often experience tribological degradation through friction and wear, which are responsible for 50–60 % of the energy loss as well as mechanical failures [8]. Therefore, there is an urgent need to develop precise, high-speed, high-torque, high-performance, safe, and durable drivetrain components. In contrast to liquid lubricants, solid lubricants are more suitable for moving components working under harsh conditions due to their superior chemical stability and environmental friendliness [9,10]. In fact, dense, uniform, and large-area solid lubricants deposited by vacuum vapor deposition techniques are very useful in improving the quality and lifespan of industrial components [11].

Graphene has garnered increasing research interest for tribological applications due to its high strength, easy shearing, low surface energy, easy dissipation, impermeability, and chemical stability [12–15]. The micro/nanoscale frictional properties on nearly perfectly smooth and tiny graphene surfaces have been studied by atomic force microscopy (AFM) and the micro/nanoscale friction properties and mechanisms have been discussed [16–20]. Macroscale graphene has been applied to bearings, gears, and seals [21], and the external effects of pressure, temperature, humidity, and adsorption molecular on the lubrication mechanism of graphene lubricants are quite complex [22]. Recently, while some reviews have summarized the macroscale lubrication of graphene solid lubricants [23–28], comprehensive overviews of its structural properties, lubrication mechanisms and applications are still lacking.

Recent advances in large-scale graphene fabrication, coupled with the development of ultra-sensitive devices detection technologies, has enabled the exploration and precise measurement of superlubricity [29,30]. Structural superlubricity refers to the state where friction is nearly zero due to the counteraction of lateral forces between atoms of two ideal, flat, rigid crystalline surfaces that slide each other in an incommensurate manner [31]. This superlubricity state is subsequently characterized by a sliding coefficient of friction (COF) less than 0.01 [32]. For example, carbon nanotubes exhibit superlubricity on the centimeter lengths, but exhibit a scale limit in the nanometer range in two dimensions perpendicular to the axial direction [33]. Building on the pioneering work of Motohisa Hirano's group at Japan's Interdisciplinary Research Laboratories [32], Quanshui Zheng's group at Tsinghua University [34], and Martin Dienwiebel's group at Leiden University [35],

* Corresponding authors.
E-mail addresses: xiaos@scut.edu.cn (S. Xiao), paul.chu@cityu.edu.hk (P.K. Chu).

https://doi.org/10.1016/j.triboint.2024.109896
Received 31 December 2023; Received in revised form 7 June 2024; Accepted 16 June 2024
Available online 17 June 2024

systems with micro/nanoscale superlubricity containing graphene/-graphene, molybdenum disulfide (MoS_2)/MoS_2, inhomogeneous graphene/MoS_2, and graphene/hexagonal boron nitride (h-BN) have been observed [36–38]. However, adsorbates, edge defects, and deformations can impact superlubricity through induced disorders, limiting the macroscale research progress [39]. A milestone came from Ali Erdemir's group at Argonne National Laboratory in 2015 with the constructing of incommensurate graphene, diamond nanoparticles, and diamond-like carbon (DLC) spheres interface can yield macroscale superlubricity [40]. Subsequently, Jianbin Luo's group at Tsinghua University, and Li Ji's group at the Lanzhou Institute of Chemical Physics further advanced the research on graphene macroscale superlubricity [41,42]. While reviews have detailed developments for structural superlubricity across scales, the macroscale superlubricity and mechanisms of graphene solid lubricant are still not well understood [43]. Furthermore, the superlubricity mechanism differences between micro/nanoscale and macroscale. For instance, tribofilm reduces friction on the macroscale, but increases friction on the microscale in the form of enhanced adhesion [13]. This is because microscale friction mainly depends on the atomic contact area changes in contrast to macroscale friction that emerges from the interactions at the interface and surface properties [44]. Considering only a few friction-reducing mechanisms at the micro/-nanoscale is insufficient for industrial applications given the complex interplays between variables cross-scale involved. Therefore, a good understanding of superlubricity mechanisms on both scales is imperative to applications for harsh working conditions.

Controlling the fabrication of large-area and high-quality graphene is expected to realize macroscale superlubricity applications. Traditional "top-down" synthesis methods like mechanical and chemical exfoliation and epitaxy are, however, inefficient and prone to contamination [45–47]. Alternatively, chemical vapor deposition (CVD) provides a viable route to produce extensive, uniform graphene in a controlled manner [48]. However, differences in CVD equipment and deposition parameters can affect defects, impurities, wrinkles, and sizes, impacting superlubricity performance [49]. Therefore, it is important to fathom how the CVD thermodynamic and kinetic influence the interfacial structure and tribological properties. In this review, the relationship between the graphene surface/interface structures and tribological properties is analyzed. Additionally, the development of macroscale superlubricity and the mechanism behind the across-scale superlubricity of graphene solid lubricants are described. Furthermore, the potential application of graphene solid lubricant focusing on components working under harsh conditions and the key factors of graphene growth structure and tribological properties by CVD technology are summarized. Finally, the challenges facing graphene solid lubricants and future research directions for engineering applications are discussed.

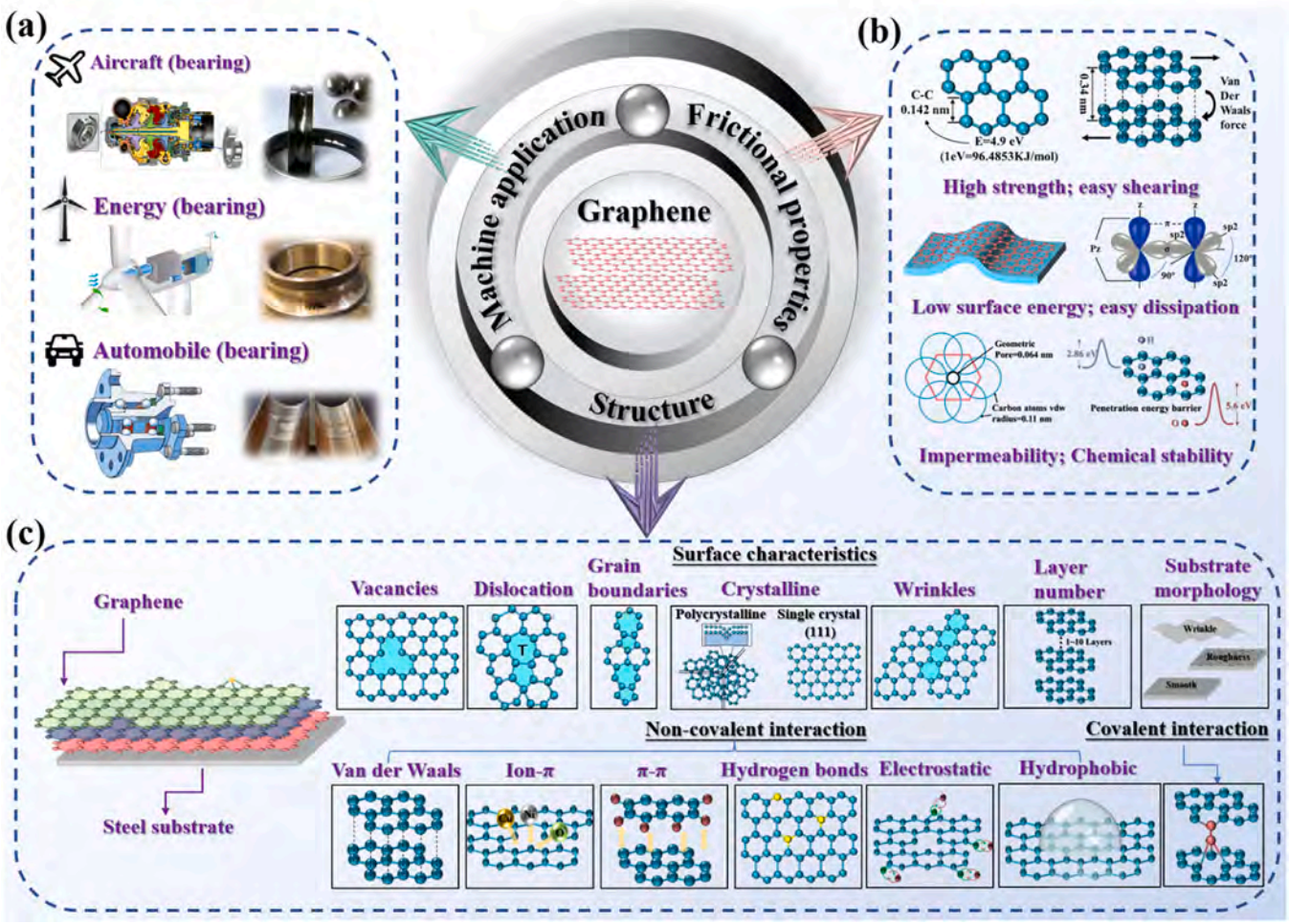

Fig. 1. An overview of graphene solid lubricants: (a) Potential application of bearings in fields such as aircrafts, energy components, and automobiles; (b) Mechanical properties such as high strength, easy shearing, low surface energy, easy dissipation, impermeability, and chemical stability; (c) Surface characteristics and interfacial non-covalent and covalent interactions. [(a) adapted with permission from Ref. [2], copyright 2023, Elsevier, Ref. [3], copyright 2019, MDPI, Ref. [4], copyright 2012, Elsevier, Ref. [5], copyright 2022, Elsevier, Ref. [6], copyright 2020, MDPI, Ref. [7], copyright 2020, TTP].

2. Structural effects on frictional properties of graphene solid lubricants

Graphene has excellent mechanical properties but the graphene surfaces and interfaces impact the friction properties. Surface defects, grain boundaries, crystallinity, wrinkles, number of layers, substrate roughness, and interfacial covalent or non-covalent interactions influence tribological characteristics. A thorough analysis of surface and interface structure, and how these relate to friction can help optimize graphene design in macroscale lubrication applications.

2.1. Frictional properties of graphene

Graphene has ideal frictional properties including high in-plane strength [12], low shear strength [13], high surface area [50], high thermal conductivity [14], and impermeability [15], as shown in Fig. 1b. This stems from the crystalline perfection with no defects, vacancies, or pores [51]. The geometric structure, energy calculation, and mechanical parameters are discussed in this section.

Graphene has the honeycomb atomic arrangement with sp^2 hybridized carbon atoms forming a two-dimensional (2D) planar structure. The electronic configuration of carbon is $1s^2 2s^2 2p_x 2p_y$, with two electrons in the 1 *s* orbital and two paired electrons in the 2 *s* orbital, while the remaining two electrons occupy the 2*p* orbitals [52]. The similar energies of the 2 *s* and 2*p* orbitals induce hybridization and free electron motion. Specifically, the 2 *s* orbital hybridizes with the $2p_x$ and $2p_y$ orbitals, producing three equal sp^2 hybrid orbitals separated by 120° and forming σ bonds. Additionally, the remaining p_z orbitals stack perpendicularly and form weak π bonds between neighboring carbon atoms [53]. Graphene also possesses high thermal conductivity due to heat transport by delocalized π electrons. [54]. The weak van der Waals (vdW) interaction between in-plane and out-of-plane carbon atoms (~2 eV/nm between layers) enables easy shearing under forces [55]. Microscale measurements have revealed several key structural parameters of graphene such as an interlayer thickness of 0.34 nm, a hexagonal carbon unit cell of 0.05 nm^2, and an areal density of 0.77 mg/m^2 [56]. Because of its lightweight, less than 4 g of graphene can cover a soccer field, which can minimize direct contact between friction interfaces. The C-C bond length in graphene is 0.142 nm, with a lattice constant of 0.246 nm and a vdW radius of 0.011 nm [57]. Consequently, the diameter of the hexagonal carbon rings is only 0.064 nm. Being just larger than hydrogen (0.053 nm) and helium (0.028 nm) molecules, this small dimension allows graphene to effectively block even the smallest gas molecules from diffusing, giving rise to high interlayer chemical stability [58]. Mechanical tests have demonstrated outstanding structural stability including the C-C bond strength of 4.9 eV, breaking strength of 43 N/m, in-plane strength of 130 GPa, and Young's modulus of 1 TPa [59]. These properties, together with the small dimension of 0.064 nm for carbon rings provide high energy barriers against atomic/molecular penetration or bond rupture, as evidenced by calculations showing barriers of 11 eV and 5.6 eV for helium and oxygen respectively [60,61]. The unique structural and frictional properties of graphene produce outstanding lubrication.

2.2. Surface/interface structure and frictional properties of graphene

In reality, graphene often contains surface defects like vacancies, dislocations, and grain boundaries introduced during fabrication or from the environment [62]. It may thus have polycrystalline, wrinkling, and different thickness and roughness. Additionally, graphene can form non-covalent interfacial interactions including vdW, ion-π, π-π stacking, hydrogen bonding, and electrostatic forces with other materials and molecules, as well as covalent interfacial interactions via chemical bonding, as shown in Fig. 1c [63]. These factors introduce complexity and heterogeneity into practical graphene systems, significantly impacting their mechanical properties and friction behavior. Therefore, a thorough grasp of structural features and interfacial interactions is critical.

The thermal conductivity is impacted by various structural factors including the number of layers, defects, edge morphology, roughness, and grain boundaries. The number of layers influences the conductivity that decreases with additional layers due to interlayer phonon scattering [64,65]. For example, the thermal conductivity decreases from 2800 to 1300 W/mK from bilayer to four-layer graphene [66]. Surface defects and edge perturbations can impact phonon transportation. Defects scatter heat flow and the thermal conductivity declines from 1800 to 400 W/mK with increasing vacancy defects [67]. Zigzag edges have higher curvature and irregularity favorable to boundary scattering compared to armchair edges [68,69]. Edge roughness and grain boundaries below the phonon mean free path likewise decrease the conductivity by phonon scattering. [70,71]. These factors impair the ability of graphene to dissipate heat under high-temperature friction conditions and influence its performance as discussed in Section 4.1 with regard to the macroscale friction applications at elevated speeds and temperatures.

The elastic modulus and tensile strength are affected by the defect density, spacing, grain boundaries, and grain size [72,73]. The defect density substantially reduces the modulus more than individual defects, as demonstrated by that a large defect density decreases the modulus, which is also correlated with the defect position and spacing being lower near stressed regions [74–76]. The strength notably decreases when defects are in proximity due to interactions between defects. [77]. Polycrystalline graphene exhibits greater temperature and strain sensitivity than single-crystalline graphene on account of its lower strength [78,79]. Moreover, strength is lower in small-grained material as small grain sizes cannot accommodate strained heptagons compared to large grains. [80,81]. Therefore, graphene is prone to friction damage under heavy loads, a topic that will be covered in Section 4.2.

The excellent chemical stability and impermeability of graphene depend on various structural factors including defects, adsorbates, dangling bonds, and wrinkles [82,83]. Defects, vacancies, and dangling bonds readily absorb metal/non-metal atoms and functional groups such as hydroxyl, carboxyl, and oxygenated groups to enhance the local reactivity via ion-π interactions [84–87]. Furthermore, severe wrinkling increases the reactivity of graphene, and large curvature areas exhibit enhanced reactivity when the ratio of the wrinkle height to radius exceeds 0.07 [88]. Impermeability mainly depends on the wettability and ionic interactions [89]. Rough substrates and wrinkles lower the water contact angle to improve impermeability, and negatively charged ions interact electrostatically to enhance the hydrophobicity, while positively charged ions decrease the surface charge and weaken impermeability. [90,91]. These structural factors influence the chemical reactivity and physical properties of graphene under special tribological environments such as vacuum, inert gas, or electromagnetic fields, as discussed in Sections 4.3 and 4.4.

2.3. Interfacial interaction and frictional behavior of graphene

The frictional properties are largely governed by interfacial interactions including strong chemical interactions and relatively weaker interactions. Strong chemical interactions include chemical adsorption reactions where atoms or molecules form strong chemical bonds with graphene, are particularly prevalent in materials such as oxidized graphene and fluorinated graphene [92,93]. These interactions significantly enhance friction force by effectively 'locking' the graphene onto substrate or counterparts. For instance, Li et al. have observed ninefold increase in friction force in fluorinated graphene compared to pristine graphene, attributed to intense localized charges at fluorine sites inducing interface potential corrugations [94]. This observation aligns with findings from Zeng et al., who have reported that fluorination enhances out-of-plane stiffness and interface potential corrugations, thereby strengthening interfacial interactions during sliding [95].

Similarly, Ko et al. have reported a sevenfold increase in friction force in oxidized graphene relative to pristine graphene, a consequence of increased out-of-plane elasticity due to oxygen-induced atomic chemical modifications on the graphene surface [96]. Weaker interactions such as vdW, π-π, and ion-π interactions allow for less resistance and provide better lubrication because the contacts are not as rigid [97,98]. This can result in lower contact resistance beneficial to smooth sliding [13,99]. Non-covalent interactions such as hydrogen bonding, electrostatic, and hydrophobic interactions also impact friction. For instance, hydrogen bonding in defective graphene facilitates the formation of C-H bonds with carbon atoms at defect edges, which passivates the friction interface, thereby mitigating strong interactions, and concurrently enhancing both chemical stability and wear resistance [100–102]. Electrostatic interactions play a key role in determining the friction between graphene and charged materials, while hydrophobicity can impact liquid environment friction properties, as verified by the positive correlation between the number of interface chemical bonds and frictional force [103,104]. Therefore, the collective effects of various interfacial interactions dictate the tribological response.

Studies in different environments have revealed strong influences by atmospheric molecules. Berman et al. have studied the macroscale friction of single-layer graphene in hydrogen (H_2) and nitrogen (N_2) atmospheres and revealed that H_2 passivates dangling bonds in fractured graphene to improve the structural stability and lubrication, but this phenomenon is not observed with N_2. [101]. Li et al. have examined the friction in air and N_2 and found that the environment influences characteristics by passivating edge defects and interlayer forces with the aid of water molecules [105]. Severe oxidation can lead to mechanical interlocking at friction interfaces, thereby reducing interlayer sliding and increasing adhesion wear, as reported by Xiao et al. [106]. Liu et al. have produced graphene oxide (GO), pristine graphene (PG), and fluorinated graphene (FG) coatings with diminishing hydrophilicity and discovered that FG coatings have the lowest friction attributable to reduced interlayer interactions from fluorine-induced repulsion [107]. The weak van der Waals forces between bilayers enable easy top-layer sliding and improve the stability as observed by Dwivedi et al. [108]. Jia et al. have observed that superlubricity originates from extremely weak interfaces [109]. Compared to uniform interfaces, vdW heterointerfaces handle twisted contacts better with significant lubrication [43,110]. Notably, the interfacial chemistry affects friction by controlling attraction and contact areas between sliding layers. A thorough understanding of the relationship between interfacial interactions and friction is crucial to advanced tribo-chemical systems.

3. Research progress and mechanism of superlubricity in graphene

Achieving “zero” friction and wear has been a long-term goal for ensuring mechanical component durability. The superlubricity from micro/nano to macroscales has garnered research interest. The timeline of key breakthroughs in cross-scale superlubricity and macroscale superlubricity of graphene is illustrated in Fig. 2. The micro/nano and macroscale superlubricity mechanisms are discussed in this section.

3.1. Cross-scale development of superlubricity in graphene

Early research focused on establishing superlubricity between two atomically clean incommensurate planes to address the cross-scale challenge. Pioneering work by Martin Dienwiebel’s group in 2004 explored the relationship between the relative rotational angle and friction of graphite/graphite thin films leading to the concept of incommensuration lattice contact and nanoscale structural superlubricity [35]. The friction is influenced by the atomic matching of interlayer planes as the contact area increases. The friction spike phenomena occurs at 0° and 60° commensurate contact states, whereas friction approaches zero for the incommensuration states. Müser et al. have observed that superlubricity is limited to the nanoscale due to symmetry and dimensions [111]. Not until 2012 did Quanshui Zheng’s group confirmed the existence of microscale superlubricity through shear-induced graphite exfoliation, where two graphite mesas with single crystalline surfaces exhibited self-retracting behavior during sliding due to clean contact interfaces [34]. This self-retraction depends on the incommensuration interlayer atomic arrangements and hexagonal symmetry, thus yielding shear forces three orders lower in any extension direction versus locked directions. Subsequently in 2013, Zhang et al. have produced centimeter-long double-walled carbon nanotubes (DWCNTs) with the pristine atomic structures, employing a silicon (Si) nanowire cantilever to verify the intershell zero friction to experimentally support macroscale superlubricity [112]. The incommensuration intershell contact is independent of length, such that during pulling, the inner shell inherently self-retracts into the outer shell to produce inherent superlubricity.

Significant progress has been made in achieving macroscale superlubricity. Pioneering work by Ali Erdemir’s group in 2015 proposed modifying the contact geometry by observing graphene preferentially rolling around diamond nanoparticles on DLC surface, thus opening new avenues for graphene macroscale superlubricity research [40]. This is due to graphene patches forming nanoscrolls around diamonds to decrease contact area, and sliding on DLC surfaces to maintain incommensurate contact. Subsequently, Saravanan et al. in 2016 leveraged highly extended layer-by-layer deposition to fabricate polyethyleneimine (PEI)/GO films exhibiting ultra-low coefficient of friction (COF) below 0.01 due to the formation of carbon nanoballs [113]. Gong et al. in 2017 have combined pulsed current plasma CVD and mid-frequency non-equilibrium magnetron sputtering to synthesize graphene sheets and MoS_2 (GL/MoS_2) thin films, where the nano-stratified structure not only lowers the contact area but also modulates the interlayer interactions to achieve macroscale superlubricity with COF of 0.004 in humid air [114]. Li et al. in 2018 have decomposed large contact areas into numerous discrete contacts through multilayered graphene nanoflakes (MGNFs) and realized transient macroscale superlubricity with COF as low as 0.001 [115]. Building upon this, Berman et al. in 2019 prepared graphene/ Fe iron nanoparticle (NP) films where "onion-like" carbon nanostructures are formed under high contact pressures and nitrogen, showing superlubricity with COF of 0.009 due to the lower interfacial adhesion friction [116]. In 2020, significant attention was directed towards graphene macroscale superlubricity. Zhang et al. have used plasma deposition to fabricate a graphene-coated plate/microsphere/sphere (GCB/GCS/GCP) superlubricity system where exfoliated graphene flakes aid microsphere rolling and contact under atmospheric and high loading conditions [117]. Androulidakis et al. have mechanically exfoliated and deposited two randomly stacked centimeters-long graphene layers to realize superlubricity through disrupted shearing and lowered interlayer shear stress [118]. Jiang et al. have prepared $MoSW_4$/graphene nanocomposite thin films by spray coatings to attain superlubricity with COF of 0.008 through the formation of friction-transforming membrane-nanoscrolls-membrane heterocontact structure in the argon (Ar) atmosphere [119]. Li Ji’s group have constructed micro-asperities topography on substrates using a femtosecond pulsed laser to achieve COF below 0.001 for 1.0×10^6 cycles under N_2 conditions with a spray-coated graphene/MoS_2 composite [42]. This is attributed to micro-asperities topography transforming macroscale contact into microscale point contact, a N_2 atmosphere pre-run that organizes the ordered interlayers, and the heterogeneous covalent/ionic of graphene/MoS_2 facilitating incommensurate contacts with weak interactions. In 2021, Huang et al. have spray-coated MXene/graphene onto silicon dioxide with a superlubricity of 0.0067 ± 0.0017 due to a protective tribofilms [120]. The following year, Li et al. have prepared graphene/SiO_2 nanocomposite coatings by spray coating. The spherical SiO_2 nanoparticles and graphene enhance macroscale superlubricity, achieving a COF ranging from 0.006 to 0.008 [121]. This enhancement

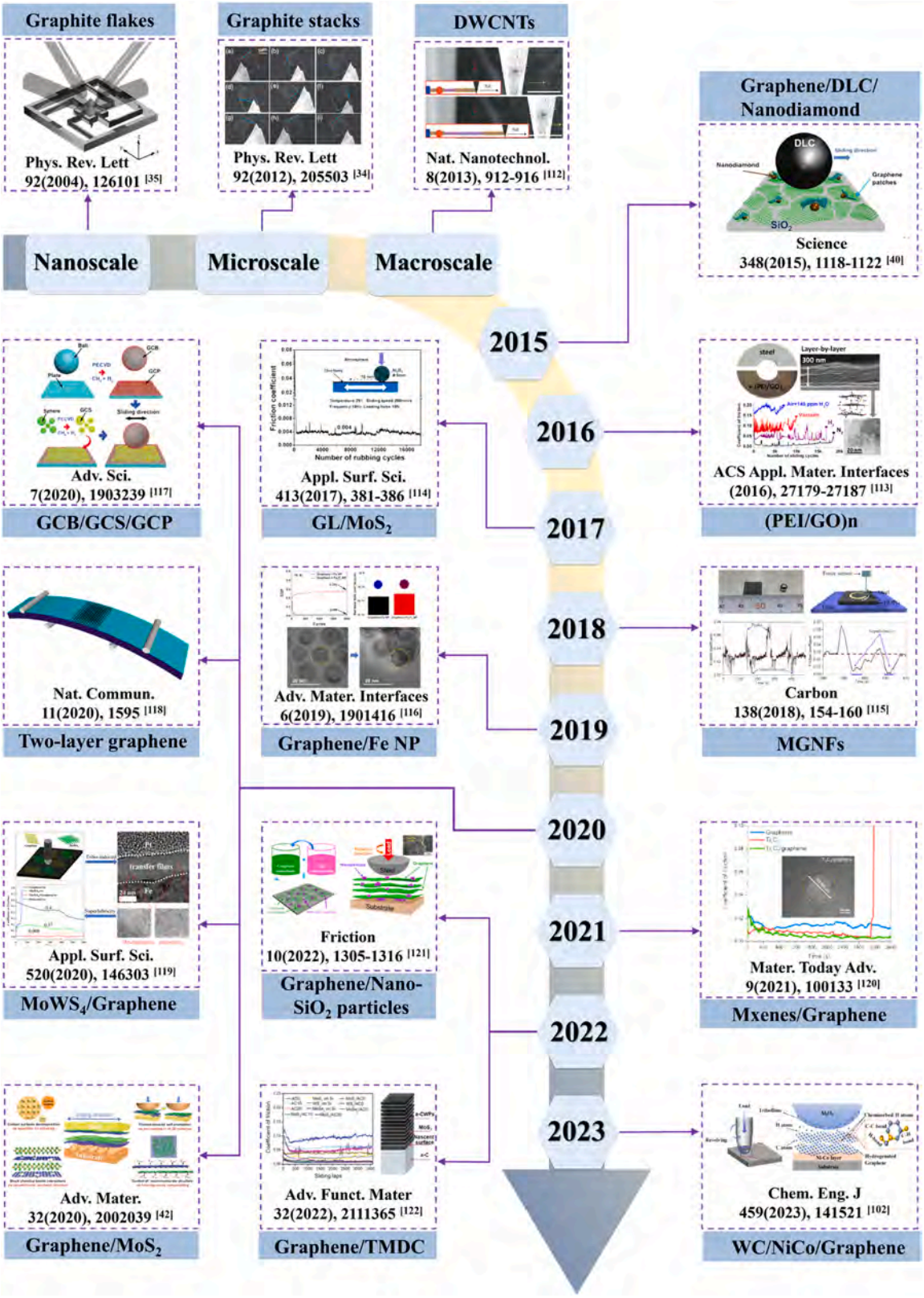

Fig. 2. Timeline of key breakthroughs in the development of superlubricity across different scales and macroscale graphene superlubricity. [Adapted with permission from Ref. [35], copyright 2004, APS. Ref. [34], copyright 2012, APS. Ref. [112], copyright 2013, Springer Nature. Ref. [40], copyright 2015, AAAS. Ref. [113], copyright 2016, ACS. Ref. [114], copyright 2017, Elsevier. Ref. [115], copyright 2018, Elsevier. Ref. [116], copyright 2019, Wiley-VCH. Ref. [117], copyright 2020, Wiley-VCH. Ref. [118], copyright 2020, Springer Nature. Ref. [119], copyright 2020, Elsevier. Ref. [42], copyright 2020, Wiley-VCH. Ref. [120], copyright 2021, Elsevier. Ref. [121], copyright 2022, Springer Nature. Ref. [122], copyright 2022, Wiley-VCH. Ref. [102], copyright 2023, Elsevier].

stems from the nanoparticles's dual role in enabling nanoscrolls through applied forces and acting as load bearers during friction process. Also in 2022, Li et al. have deposited transition metal dichalcogenides (TMDC) heterostructures of MoS_2, WS_2, and MoS onto amorphous carbon (a-C) by spinning to attain COF of 0.006 under vacuum [122]. This ultra-low friction results from the capture of wear debris between TMDC layers that polish a-C rough nascent surface, the formation of graphene/TMDC heterostructures that reduce strong interfacial interactions, and the creation of multi-point lamellar tribofilms that decrease contact area. In 2023, Fan et al. have in situ grown high-quality hydrogenated graphene coatings on WC/NiCo materials by hot filament CVD (HFCVD) with self-duration and self-healing through strong C-H bonds and chemisorbed hydrogen atoms with a COF of 0.009 under ambient conditions [102]. Representative studies from 2015 to 2023 have successfully produced graphene solid lubricant and demonstrated macroscale superlubricity using various fabrication techniques. However, most research to date has been limited to the laboratory scale under controlled dry and low-load environments. To realize the practical potential of superlubricity, further work is needed to enhance the stability and durability under more complex field conditions. It is also important to investigate across-scale superlubricity mechanisms of graphene solid lubricant to establish a robust theoretical foundation guiding macroscale applications.

3.2. Micro/nano-scale superlubricity mechanism of graphene

The atomic model and energy dissipation model provide complementary explanations for the micro/nanoscale superlubricity of graphene. The atomic model emphasizes the arrangement and interactions of graphene surface atoms and elucidates the role of atomic-scale structure and mechanics. The energy dissipation model focuses on energy transfer and dissipation across the surface, highlighting the dynamical characteristics of energy transmission and loss. An integrated understanding of these perspectives offers micro/nano-scale insights into the exceptional superlubricity of graphene.

3.2.1. Atomic model

The Prandtl-Tomlinson (PT) and Frankel-Kontorova (FK) models are essential theoretical frameworks for the atomic-scale friction mechanism. The PT model describes how a nanotip oscillates in a sinusoidal potential energy landscape. It relates the friction coefficient η to energies stored in the tip-surface interaction and restoring forces. Based on the η value, the model distinguishes between the superlubricity and stick-slip friction regimes. When $\eta < 1$, superlubricity sliding occurs, and $\eta > 1$ indicates stick-slip friction [123]. The FK model consists of a chain of harmonically coupled particles subjected to a periodic potential and introduces the concepts of commensurability ratio (Ω) and critical spring constant (k_c) [124]. When the spring constant exceeds the critical value ($k > k_c$), the model predicts a transition to a superlubricity state [125]. The PT model sheds light on the superlubricity conditions based on stick-slip regimes, and the FK model explains the superlubricity concerning structural commensurability and threshold mechanical forces. All in all, the PT and FK models enhance our understanding of the atomic-scale friction behavior by providing an important theoretical foundation.

3.2.2. Energy dissipation model

The energy dissipation model describes energy transfer and conversion by considering electron-phonon coupling, out-of-plane deformation, and non-conformal contact. One aspect is electron-phonon coupling, which refers to the interaction between lattice vibrations and electrons [126,127]. Researchers have explored modulating electron-phonon interactions through doping, choosing substrates, and altering graphene size/shape to introduce influence energy dissipation [128–130]. Both in-plane and out-of-plane deformations of graphene affect energy dissipation. In-plane deformation occurs along the lattice plane, whereas out-of-plane deformation occurs perpendicular to it. Owing to weak interlayer interactions, graphene is prone to perpendicular deformations. Therefore, suppressing these out-of-plane deformations can reduce lattice distortions and dissipation, thereby enabling superlubricity [131]. Researchers have studied controlling local deformation and relaxation using properties such as the thickness, substrate, strain, temperature, sliding rate, and functionalization to achieve micro/nanoscale superlubricity [132–135]. Additionally, incommensuration contact represents a superlubricity mechanism where non-matched atomic configurations accumulate elastic energy instead of rapidly dissipating it to reduce friction [136–139]. Both homogeneous and heterogeneous graphene systems provide pathways to realize such incommensuration superlubricity. Fig. 3 summarizes the studies of homogeneous graphene, graphene-inert metal, and heterogeneous graphene-2D material structure systems exhibiting incommensuration superlubricity. Feng et al. have studied the superlubricity behavior where the transition from commensurate to incommensurate contact between graphene nanoflakes and surface, as shown in Fig. 3a [140]. Li et al. attribute graphene superlubricity to dispersive interactions forming asymmetric interfaces between nanosheets and SiO_2 probes [141]. Similarly, Jianbin Luo's group have achieved ultra-low 0.003 friction coefficients at given relative surface rotation angles using a graphene-coated microsphere probe homogeneous graphene structure, as shown in Fig. 3b [41]. The superlubricity mechanism provides a homogeneous interface between graphene and non-layered materials for friction increases. Studies comparing the vdW forces in graphite/h-BN and graphite/MoS_2 show lower interactions for heterogeneous interfaces than graphene interlayers, as shown in Fig. 3c [142]. When graphene forms heterogeneous structures with molybdenum (WS_2) or other 2D materials, the interlayer sliding barrier is significantly lower than that in homogeneous structures, thereby facilitating mismatched incommensuration contact formation independent of sliding angles, as shown in Fig. 3d [34,143]. Kawai et al. have investigated the superlubricity of graphene nanoribbons on gold (Au) surfaces (Fig. 3e) [144], while others have examined ultra-low friction on inert metals like Pt (Fig. 3f) [145,146].

The key conditions for graphene superlubricity on the micro/nanoscale include smooth defect-free surfaces, minimal interfacial bonding, and incommensuration contact. First of all, pristine surfaces without defects or deformations are necessary to eliminate physical locking forces during sliding. Secondly, the sliding must occur between pure graphene layers with no strong chemical bonds across the interfaces. Thirdly, the contact being in an incommensurate state can further reduce atomic interactions. The synergy of these conditions serves to maximize frictional energy dissipation by minimizing mechanical hindrance, chemical bridging, and interatomic interactions, thus accounting for exceptional frictionless behavior at small scales.

3.3. Macroscale superlubricity mechanisms and influencing factors of graphene

Compared to micro/nano-scale, the macroscale superlubricity of graphene involves additional factors such as material composition, surface morphology, environmental conditions, loads, and interfacial chemistry. The macroscale superlubricity mechanisms of graphene can be summarized as i) incommensuration contact, ii) chemical reactions during tribofilm formation, self-orders sliding, and hydrogen passivation through bond formation/breaking, and iii) Microstructural transformations under stresses, including strain engineering and microbearing rolling. The correlations between those influencing factors and mechanisms of macroscale superlubricity are summarized in Table 1.

3.3.1. Incommensuration contact mechanism

Incommensuration contact mechanisms involve graphene surfaces with mismatched crystals through rotational symmetry, lateral

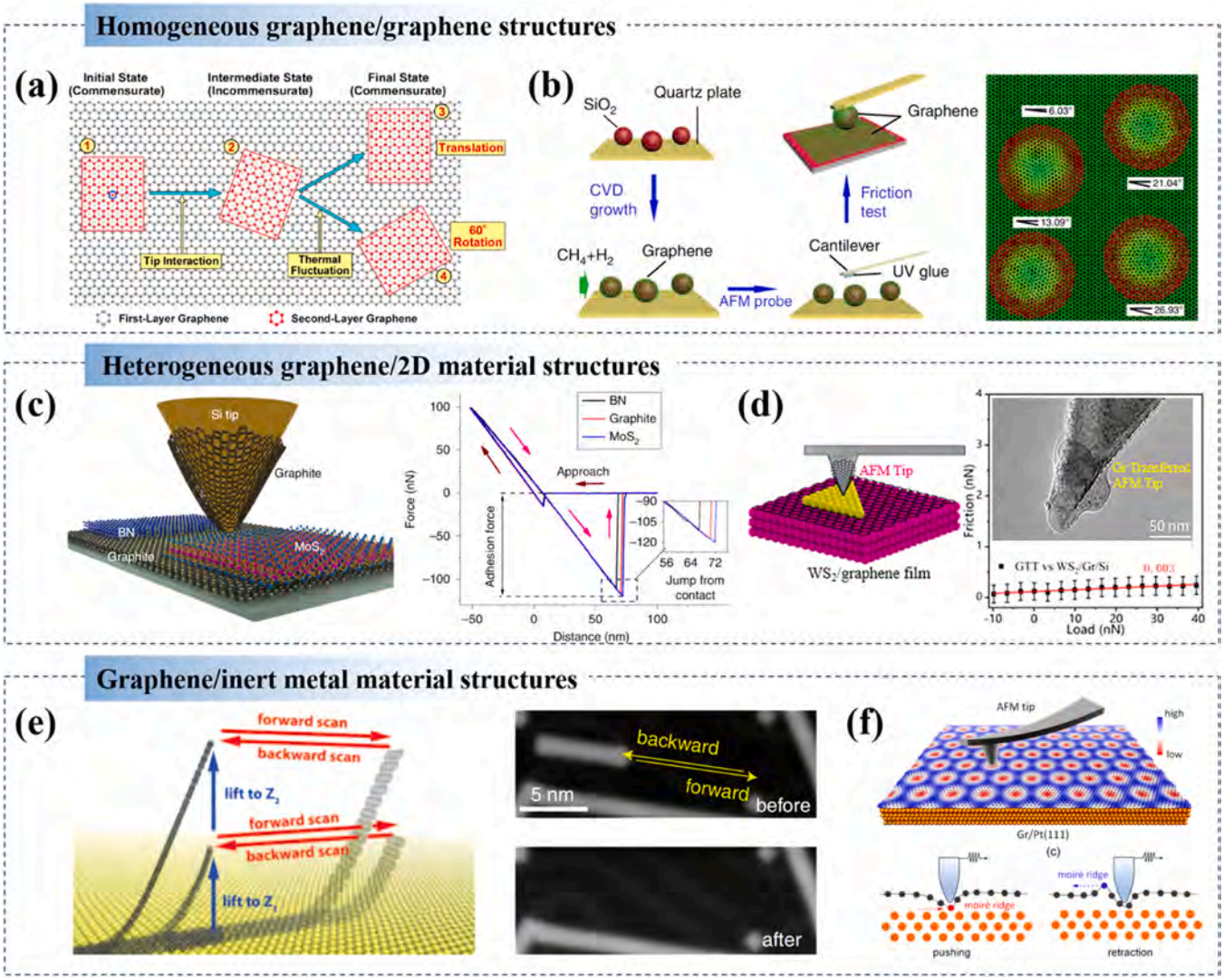

Fig. 3. Graphene superlubricity incommensuration systems: (a, b) Homogeneous graphene/graphene structure; (c, d) Heterogeneous graphene/2D materials structure; (e, f) Graphene/inert metal materials structure. [140], copyright 2013, ACS. [41], copyright 2017, Springer Nature. [142], copyright 2019, Springer Nature. [143], copyright 2020, ACS. [144], copyright 2016, AAAS. [145], copyright 2022, ACS].
(a) [(a) adapted with permission from Ref. (b) (b) adapted with permission from Ref. (c) (c) adapted with permission from Ref. (d) (d) adapted with permission from Ref. (e) (e) adapted with permission from Ref. (f) (f) adapted with permission from Ref.

Table 1
Correlations between influencing factors and mechanisms of macroscale superlubricity.

Factors	Detailed description	Mechanism
Material composition	Use of materials like graphene, DLC, MoS_2, etc. with low shear strength and mismatched lattice structures	Incommensuration contact mechanism
Surface morphology	Smooth and minimized direct contact	Microstructural transformation mechanism
Environmental conditions	Temperature, pressure, humidity and gases influence tribofilm stability	Chemical reaction mechanism
Loads	Stress-induced structural arrangement and interlayer sliding	Microstructural transformation and incommensuration contact mechanisms
Interfacial chemistry	Adjustments of interfacial interactions at sliding interface	Chemical reaction mechanism

orientation, or lattice spacing to achieve macroscale superlubricity. Androulidakis et al. have shown that randomly stacked graphene bilayers create an incommensurate state between the layers on the macroscale, which is important to superlubricity (Fig. 4a) [118]. Moreover, Li et al. have proposed micropatterning steel surfaces with graphene/MoS_2 coatings, leveraging heterogeneous covalent/ionic interaction to reduce contact and interaction between layers (Fig. 4b) [42]. This design achieves macroscale superlubricity with a COF of 0.007 in rough steel-steel friction and advances macroscale superlubriity applications for steels. In investigations of macroscale superlubricity mechanisms, researchers have identified incommensurate contact as a crucial factor influencing friction performance [40,122]. To realize wider superlubricity applications, researchers have established design standards for graphene heterostructure incommensuration mechanisms. The standards specify that heterostructures must possess intrinsic interfacial incommensuration to inhibit interlayer interactions, have low interlayer binding energy to reduce out-of-plane interferences, and exhibit high in-plane stiffness to offset interfacial deformation [125].

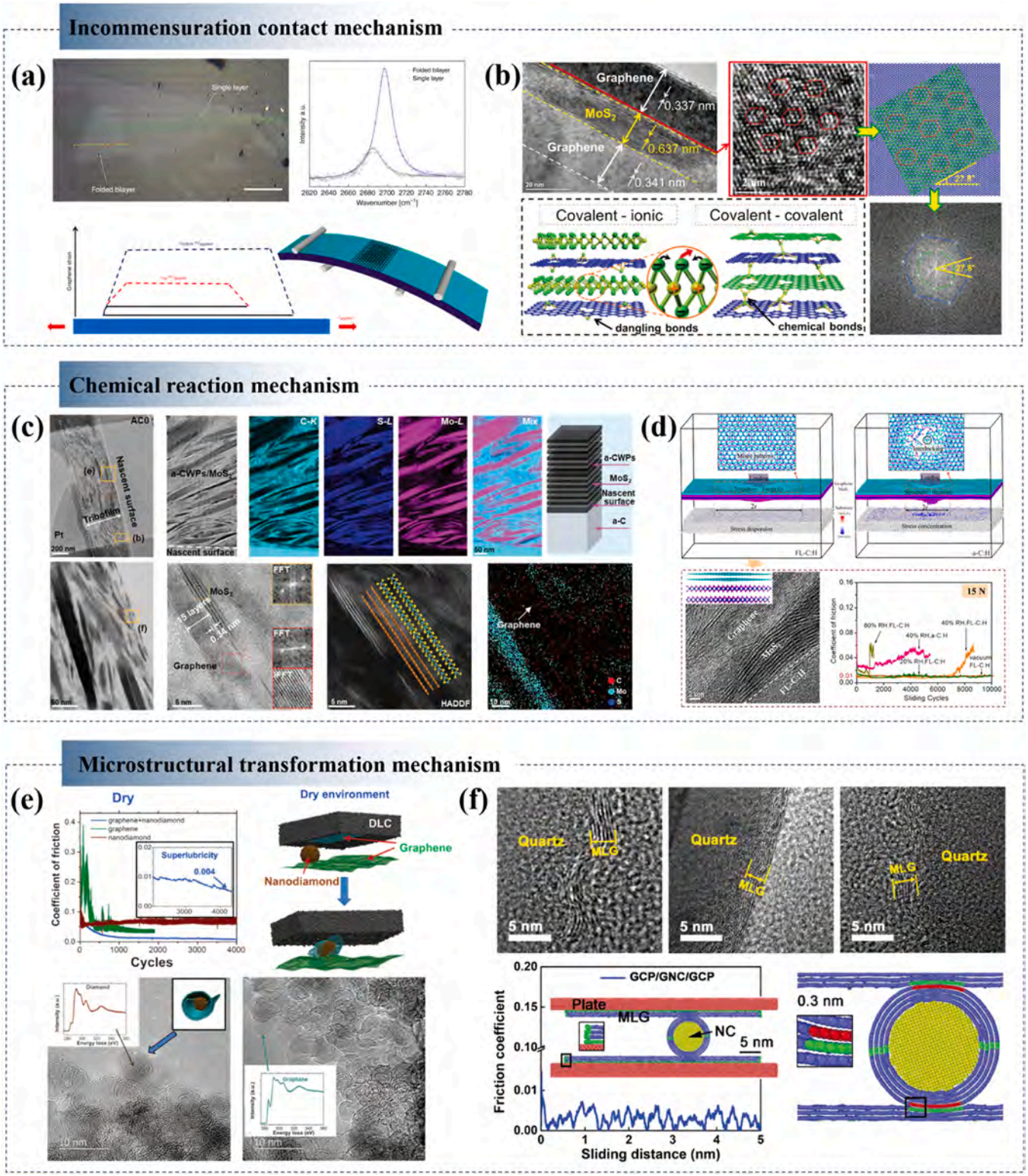

Fig. 4. Macroscale superlubricity mechanism of graphene: (a, b) Incommensuration contact mechanism; (c, d) Frictional chemical reaction mechanism and (e, f) Microstructural transformation mechanism. [118], copyright 2020, Springer Nature. [42], copyright 2020, Wiley-VCH. [122], copyright 2022, Wiley-VCH. [5], copyright 2022, Elsevier. [40], copyright 2015, AAAS. [117], copyright 2020, Wiley-VCH.].
(a) [(a) adapted with permission from Ref. (b) (b) adapted with permission from Ref. (c) (c) adapted with permission from Ref. (d) (d) adapted with permission from Ref. (e) (e) adapted with permission from Ref. (f) (f) adapted with permission from Ref.

3.3.2. Chemical reaction mechanism

Tribofilm formation is an important chemical reaction mechanism in the superlubricity process, involving interfacial oxidation and reduction during friction and generating carbon films covering the sliding interface. These films fill surface roughness, reduce direct contact, and enable macroscale superlubricity. Li et al. have studied the macroscale friction behavior of self-assembled graphene and found intermittent superlubricity between graphene and highly ordered pyrolytic graphite (HOPG) substrates with a COF of 0.001 through tribofilm formation [115]. Yin et al. have used graphene quantum dots on DLC films to realize macroscale superlubricity under high speed/load and N_2 conditions [147]. Their research shows that tribofilms containing amorphous carbon and SiO_x are key to macroscale superlubricity. Li et al. have transformed TMDC/a-C wear products (a-CWPs)/TMDC multilayers into graphene/TMDC laminated tribofilm during friction and revealed the important role of transferred graphene films in macroscale superlubricity (Fig. 4c) [122]. Additionally, self-ordered slipping mechanisms form laminated structures with negligible interfacial friction on graphene surfaces. Liu et al. have discovered that weakly chemically bonded and ordered graphene/MoS_2 interfaces promote stable macroscale superlubricity during friction [148]. Hydrogen passivation involves chemical reactions between hydrogen and graphene surfaces, which can stabilize interfaces by passivating surface defects and dangling bonds. Li et al. have achieved macroscale superlubricity from graphene/MoS_2 under a 15 N load using a stable fullerene-like hydrogenated carbon (FL-C:H) substrate, as shown in Fig. 4d [5]. Li et al. have used substrates to achieve superlubricity and other researchers have shown intrinsic interface stability through in situ hydrogen passivation. For example, Fan et al. have passivated graphene edges and bonds with hydrogen during in situ fabrication, formed strong C-H bonds within the hydrogenated graphene structure, and enabled durable macroscale superlubricity [112].

3.3.3. Microstructural transformation mechanism

Strain engineering and micro-bearing rolling play important roles in enabling macroscale superlubricity of graphene through microstructural transformation. Strain engineering modifies the lattice arrangement, spacing, and local geometry by applying external strain/deformation, allowing further control over the interface microstructure. Androulidakis et al. have demonstrated this by applying controlled tensile strain to induce misalignment, wrinkles, and incommensuration stacking to overcome the limitations of the graphene superlubricity [118]. The micro-bearing rolling mechanisms provide another pathway to facilitate macroscale superlubricity. They function by converting frictional shear stress into rolling motion through nanoscale asperity contact, thus reducing direct collisions and contacts between sliding surfaces. Berman et al. and Li et al. have combined graphene with nanoparticles to form nanoscroll structures under shear force that serve as critical load-bearing elements, as shown in Fig. 4e [40,121,149]. Additional micro-bearing rolling effects are provided by edge scrolling and encapsulation during friction. Jiang et al. have shown that $MoWS_4$/-graphene composites promote the transition to a steel/rolling layer/-steel interface during steel/steel friction [119]. Furthermore, Li et al. have discovered graphene nanoscrolls generated between graphitic and fullerene-like carbons under friction to dilute interlayer shear contact areas and realize macroscale superlubricity [150]. Zhang et al. have enhanced the superlubricity with graphene-coated microspheres that buffer the stress and prevent concentration, as shown in Fig. 4f [117].

On the macroscale, graphene's superlubricity still follows the fundamental mechanism of weak interlayer sliding. Appropriate strategies can be adopted to regulate the macroscale interface structure: (i) Constructing incommensuration structures and utilize the natural incommensurability of 2D materials to enable stable superlubricity, (ii) in situ fabrication of self-passivating graphene coatings through surface modification techniques, and (iii) Design of high load-bearing interfaces to improve the durability of superlubricity. Combining graphene with nanoparticles or dividing the substrate surface into microscale points where each point represents individual rough contact while their collection represents mesoscale contact can bridge the gap between micro-nanoscale to macroscales, thus facilitating the development and application of graphene superlubricity on the macroscale.

4. Potential applications of graphene solid lubricant under harsh working conditions

With advancement in deep-sea engineering, deep-earth exploration, aerospace exploration, nuclear energy application, and high-speed railway system, ensuring the reliable operation of mechanical components such as gearboxes, bearings, and valves under harsh working conditions—high temperature, heavy load, high speed, vacuum, and special atmospheres—has become critical [151]. Traditional liquid lubrication has limitations in these challenging environments, making graphene solid lubricant a promising solution [152,153]. Therefore, the development of high-performance graphene solid lubricants capable of withstanding harsh working conditions is of great significance for industrial applications.

4.1. Potential application of graphene solid lubricants under high speed and temperature

Operating under high speed and temperature conditions poses challenges for mechanical components. Rapid overheating at high speeds increases failures, while temperature rise degrades the geometry accuracy and accelerate wear over time. Graphene is an effective solution due to its high thermal conductivity and chemical stability. The lubricating ability under high speed and temperature conditions are shown in Table 2. Wang et al. have deposited graphene coatings on journal bearings by CVD, showing ultra-low friction even after extensive start-stop cycles attributed to stress homogenization [7]. However, wear increases linearly during thermal decomposition as covalent bonds form between dangling bonds and environmental molecules. Aliyu et al. have found that ultra-high molecular weight polyethylene (UHMWPE)/-graphene nanoplates (GNPs) reduce wear by 51 % at a speed of 1 m/s, though wear still rises with speed presumably due to amplified heat generation [154]. Others focused on improving heat dissipation. Nemati et al. have prepared polytetrafluoroethylene (PTFE)/graphene oxide (GO) composite coatings on stainless steel by spin coating, achieving an excellent COF of 0.1 and superior wear resistance at 400 ℃ due to the uniform dispersion of GO that reinforces the PTFE matrix [155]. Likewise, Wang et al. have dip coated expanded graphite (EdG)/sodium metasilicate (NSO) composites to reduce steel friction and wear by 85 % and 60 % at 850 ℃ through uniform dispersion to form protective tribofilms [156]. Shukla et al. have plasma sprayed GNPs-CeO_2 coatings that decrease friction and wear at 600 ℃ because the GNPs act as the bridge to maintain uniform tribofilms and inhibit particle fracture [157]. Enhanced oxidation and degradation resistance have been observed. Xu et al. have fabricated multi-layer (MLG)/TiAl coatings on disks using spark plasma sintering demonstrating ideal friction up to 400 ℃, a phenomenon ascribed to the ability to resist oxidation [158]. NiAl composites with graphene nanoplatelets (NAG) coatings deposited by Ibrahim et al. exhibit excellent lubrication below 400 ℃, possibly due to increased degradation at higher temperature [159]. Yang et al. have introduced composites of SnAgCu, Al_2O_3, and graphene into Ti alloy microchannels by infiltration and sintering, showing friction stability to 450 ℃ from thermal degradation resistance [160].

4.2. Potential application of graphene solid lubricants under heavy loads

Operating mechanical equipment under heavy loads presents challenges such as fatigue damage, plastic deformation, thermal effects, and increased wear failure risk. Graphene has properties like high in-plane strength and a large specific surface area that enable it effectively to

Table 2
Potential application of graphene solid lubricants under high speed and high temperature conditions.

Extreme condition	Graphene system	substrate	Synthetic method	Friction parameters	COF	Service life	Favorable factor	Negative factor	Reference
High speed	Graphene	CuAl10Fe3	CVD	Journal bearing wear tester, start-stop test, 20-22 ℃, 50 ± 5 %RH	0.00078	200 cycles	homogenization of contact stress	/	[7]
	UHMWPE/GNPs	Al	Drop casting	Mechanical engineering department (KFUPM), AISI 4140 steel disc counterface, 1-2 m/s, 0.1-1 MPa, room temperature, 59 ± 3 % RH	0.015-0.007	100 m	High mechanical thermal properties	/	[154]
High temperature	PTFE/GO	Stainless steel	Spin coating	Reciprocating tribometer, stainless steel ball, 400 ℃, 5 N, 4 mm/s, 4 mm	0.1	1000 cycle	Homogeneous dispersion	deformation	[155]
	MLG/TiAl	HT-1000	Spark plasma sintering	HT-1000 ball-on-disk tribometer, Si_3N_4 ball, Ø 6 mm, 0.2 m/s, 400 ℃, 10 N	0.36	/	High conductivity	oxidation	[158]
	NAG	NiAl	Spark plasma sintering	HT-1000 ball-on-disk tribometer; Si_3N_4 ball; Ø2 mm , 0.2 m/s; 12 N , 400 ℃	0.25-0.6	/	Tribofilm	Stress concentration	[159]
	EdG/NSO	Mild steel	Drop casting	Bruker UMT Tribolab tribometer, high speed steel ball, Ø6.35 mm, 850 ℃, 10 N , 0.094 nm	0.08	900 cycles	Tribofilm	/	[156]
	CeO_2/GNPs	Gritblasted steel	Plasma sprayed	TR-20LE-CHM800 tribometer, WC ball, Ø6 mm, 40 N, 250 rpm, 600 ℃	0.25-0.35	/	Uniform tribofilm	Three body wear	[157]
	SnAgCu/Al_2O_3/Graphene	Ti alloy	Spark plasma sintering	MFT-5000 tribometer, Si_3N_4 ball, Ø6 mm, 50-55 %RH, 0.2-0.35 m/s, 450 ℃, 16 N	0.22-0.26	/	Inoxidizability	peeling	[160]

disperse stresses, form protective layers, and bear loads, as shown in Table 3. Garcia et al. have applied a CHCl/ethylene glycol/graphene composite coating on steel by drop casting [161]. Owing to the low shear strength, the coating exhibits low friction (0.01) and a long lifetime exceeding 12,633 m under a heavy load. Yin et al. have deposited graphene quantum dot (GQD) modified DLC films on steel bearings using ion plasma and solution methods [147]. The coatings achieve superlubricity under a load of 1.61 GPa and dry nitrogen as GQD degradation forms amorphous carbon transfer films. Lu et al. have fabricated graphene nanoplatelets reinforced Ni_3Al metal matrix composites (GNMMCs) using laser deposition [162]. The incorporation of GNPs confers increased plastic deformation resistance, allowing deformation to progressively expand from coarse to fine grains under high compressive loads to maintain excellent wear resistance. Wang et al. have drop casted Na_2Co_3-graphene coatings on steel discs and provided effective lubrication under a 2.06 GPa load ascribed to its strong adhesion, friction film formation, and high load-bearing capacity [163]. Wu et al. have prepared TiO_2-reduced graphene oxide (TiO_2 @RGO) reinforced polyimide composites and found that the wear rates decrease to one-tenth of pure polyimide under 300 N loads [164]. This is because the large surface area of the graphene nanosheets enables the formation of compressible/elastic nanoclusters. Incorporating graphene in various forms exploits its stress-dissipating, tribofilm-forming, and interface-reinforcing properties consequently enhancing the performance of mechanical components under heavy loading conditions.

4.3. Potential application of graphene solid lubricants under vacuum and nitrogen environment

High-pressure forging, nuclear engineering, and space exploration equipment in harsh environments such as high vacuum, inert gases, and external fields present challenges. The high in-plane strength, chemical stability, and resistance to degradation in vacuum and N_2 environments make graphene a potentially promising lubricating material, as shown in Table 4. However, the interlayer chemical interactions can concentrate stress and cause delamination. Li et al. have deposited graphene/MoS_2 heterostructures on carbon substrates by spraying [5]. These coatings exhibit superlubricity in vacuum, attributed to the high elastic deformation that disperses stresses and the absence of environmental water molecules. Further explaining the negative effect of water molecules, they enhance chemical interactions at the graphene friction interface, leading to a pinning effect between graphene and environmental molecules. This effect impedes lubrication by favoring interlayer adhesion over sliding, consistent with the findings of Arif et al. [165]. Shi et al. have deposited graphene/DLC coatings on Si and steel by magnetron sputtering and spraying [166]. The resulting microstructural changes such as scrolling, micro bearings, and asymmetric shear enable low friction in vacuum. Berman et al. have chemically transferred graphene to stainless steel and observed low friction due to the protection inhibiting oxide/nitride formation at sliding interfaces in vacuum and N_2 environments [167]. Yang et al. have self-assembled SiO_2 modified GO on Si and PTFE substrate, which exhibits outstanding lubrication in N_2 and leverages mechanisms such as shielding, self-lubrication, rolling, sliding, and embedding at the friction interface [168]. It is noted that vacuum and nitrogen environments can sometimes adversely affect the lubrication performance of graphene coatings. The coatings excel in the presence of oxygen and water molecules, which can passively interact with edge dangling bonds and defects to reduce friction [105]. For instance, Wang et al. have fabricated metal ion (Al^{3+}, Cu^{2+})-modified graphene coatings on steel by spin coating and found that graphene lubrication performs well in air but fails in vacuum without passivation [169]. Notably, Al^{3+} can enhance adhesion, load transfer, and graphene site passivation to further improve graphene lubrication in vacuum.

Table 3
Potential application of graphene solid lubricants under high load conditions.

Extreme condition	Graphene system	substrate	Synthetic method	Friction parameters	COF	Service life	Favorable factor	Negative factor	Reference
High load	ChCl/ethylene glycol/ graphene	H-60 SAE O1 Steel	Drop casting	CETR-UMT-2 tribometer, 22 ℃ , 50 %RH, 120 N	0.01	12633	Low shear strength	/	[161]
	GODs/DLC	Bearing steel	Ion vapor deposition and chemical solution method	TRB3 tribometer, 1.61 GPa, 15 cm/s, N_2, bearing steel ball, Ø6 mm, 20 ℃	0.014	45 m	Tribofilm	Covalent bonds	[147]
	GNMMCs	Ni_3Al alloy	Laser melt deposition	MFT-5000 tribometer, Si_3N_4 ball, Ø6 mm, 30 N, 35-55 %RH, 0.2 m/s	0.3	1000 m	Deformation strength	Peeling	[162]
	Na_2CO_3/ graphene	316 stainless steel	Drop casting	Bruker UMT tribometer, stainless steel ball, 22.5 ± 1.5 ℃, RH 60 ± 2 %, 2.06 GPa, 0.094 m/s, 15 mm	0.3	/	Stronger adhesion, soft tribofilm	/	[163]
	TiO_2 @RGO	PI stainless steel	Drop casting spray deposition	Ring model and wear tester, 0.42 m/s, 300 N, 23 ℃, 20 ± 5 %RH	0.23	/	High specific surface area, nanocluster, tribofilm	/	[164]

Table 4
Possible application of graphene solid lubricants under vacuum, N_2, electric, or magnetic conditions.

Extreme condition	Graphene system	substrate	Synthetic method	Friction parameters	COF	Service life	Favorable factor	Negative factor	Reference
Vacuum	MoS_2/ Graphene	FL-C:H and a-C:H	Spraying	UMT-3 tribometer, vacuum, room temperature, steel balls, Ø3 mm, 9.42 cm/s, 15 N, 5 mm	0.009	10,000 cycles	Stress dispersion	Water molecule	[5]
	GO-Al^{3+}	SAF 2507	Spin-coating	CSM vacuum tribometer, AISI 52100, bearing steel ball 0.25 N, 10 mm/s, 20 %RH, 5 mm, 5×10^{-5} mbar vacuum	0.2	3600 cycles	Passivation	Chemical reactivity	[169]
	Graphene/ DLC	9Cr18	Magnetron sputtering and spraying method	UMT-3 high vacuum tribometer, 5 × 10-5 mbar vacuum, 9Cr18 bearing steel ball, Ø6 mm, 1 N, 500 r/min.	0.05-0.15	1696 m	Micro-bearing	Flaking	[166]
Vacuum/ N_2	Graphene	400 C Stainless steel	Chemical exfoliation	CSM high vacuum tribometer, N_2, 2 N, 9.4 cm/s, vacuum	0.15-0.3	600 cycles	Low shear	/	[167]
N_2	GS-PTFE	Si and PTFE	Self-assembly	TRB3 ball-on-disk tribometer, 1 N, 27 ℃, 22 %RH, PTFE and GCr15 ball, N_2	0.2	8400 cycles	High mechanical strength	flaking	[168]
Electric field	GNC	Si	ECR plasma sputtering system	Ball-on-plate tribometer, GCr15 ball, Ø6.35 mm, 3 N, 5 mm/s, 20 mm, 23-26 ℃ , 30-40 %RH , 0.5 A	0.03-0.05	/	Tribofilm, electron transport channel	peeling	[170]
	Cu/ graphene	H65 Brass	Drop casting	Ball-on-flat, H65 Brass contact pair, 25 ℃ , 60 ± 10 %RH , 2 N, 3 mm, 0.2 A, 1 A, 2 A, 3 A	0.17-0.2	/	Expan graphene	Friction-induced vibration	[171]
Magnetic field	MGO	Galvanized sheets	Drop casting	HSR-2 M tribometer, GCr15, Ø6 mm, 3 N, 220 rpm, 0 mT, 20 mT, 40 mT	0.121	/	Tribofilm adhesion	/	[172]

4.4. Potential application of graphene lubricant under electric and magnetic conditions

In the evolution of electromechanical systems, the quest for materials that can provide efficient lubrication under the influence of electric or magnetic fields is pivotal. Graphene, with its exceptional electrical properties and thermal conductivity, emerges as a promising candidate to address these challenges, as shown in Table 4. Sun et al. have deposited graphene nanocrystalline carbon (GNC) films on silicon by electron/ion beam irradiation and revealed that those films have high conductivity, shortened running-in periods, and reduced electrical/ mechanical energy consumption [170]. Additionally, the accumulation of rapidly transferred carbon debris at the interface plays a crucial role in achieving low friction. Wang et al. have drop casted graphene coatings onto brass to decrease the friction coefficients and contact resistance since larger currents suppress friction-induced vibrations [171]. Specifically, the reduced contact pressure and more uniform pressure distributions in high currents allow graphene coating expansion and enhance the contact with counterparts and expression of conductivity and lubrication properties. Bai et al. have chemically grafted Fe_3O_4 nanoparticles onto magnetized GO (MGO) and deposited them on galvanized sheets [172]. The inclusion of Fe_3O_4 nanoparticles augments the adhesion capabilities when exposed to magnetic fields, which in turn bolsters the anti-friction properties.

In summary, traditional liquid lubricants fall short in extreme environments characterized by high temperature, heavy load, high velocity, vacuum, and other specialized conditions. As discussed, graphene solid lubricants effectively reduce friction at macroscale application and expand the lubrication boundaries of equipment operating under harsh conditions. However, to broaden the stable industrial application of graphene solid lubricants under actual working conditions, key issues need to be addressed. These include developing methods to enhance the bonding strength, load capacity, and durability of in-situ deposited graphene coatings on industrial substrates. Additionally, understanding

the effects of harsh operating conditions on the lubrication performance and mechanisms is crucial for controlling the industrial-grade graphene superlubricity.

5. CVD synthesized graphene solid lubricant for tribological properties

Using controlled CVD methods to grow high-quality and large-area graphene solid lubricants with superlubricity and durability is key to macroscale applications under harsh working conditions. Given the sensitivity of tribological properties to the surface structure, layers, size, crystallinity, and chemical properties of graphene must be controlled. This is a guide for graphene solid lubricant synthesis to realize durable lubricity systems in a controlled manner.

5.1. Design and features of CVD equipment

There are three main steps in the CVD process of thin film growth: (i) transport of reactants, (ii) chemical reaction, and (iii) removal of reaction by-products [173]. CVD equipment involves a gas transport system that delivers gaseous reactants in a controllable manner, a reaction chamber system and vacuum system that provide an enclosed chemical reaction environment, an energy system that provides energy for the chemical reaction, an automatic control system that controls the reaction pressure and gas discharge, and a waste gas treatment system. CVD can be categorized based on the reaction pressure: atmospheric pressure CVD (APCVD), low-pressure CVD (LPCVD), and ultra-high vacuum CVD (UHVCVD) (Fig. 5a) [174]. LPCVD and UHVCVD produce better graphene film quality than APCVD due to reduced side reactions and more uniform precursor concentration [175]. A lower pressure also improves the growth efficiency and thickness uniformity on large areas. To provide the high temperatures required for graphene growth, common heating methods include hot wall CVD (HWCVD), cold wall CVD (CWCVD), and HFCVD, as shown in Fig. 5b. In HWCVD, resistive heating of the entire reactor allows temperatures over 1000 ℃ but the long ramping time from room temperature limits the efficiency [176]. Additionally, deposited contaminants flaking from heated walls impact the uniformity. To address these issues, CWCVD has been proposed to selectively heat the substrate instead of the whole system and reduce the ramping time significantly. [177]. However, larger temperature differences between the substrate and walls can cause non-uniform deposition. CWCVD using heating methods such as magnetic induction or halogen lamps can improve the efficiency but quality control still relies on HWCVD.

Resistively heated HWCVD is the most common method In HFCVD, the precursors such as carbon and hydrogen gases are decomposed at the

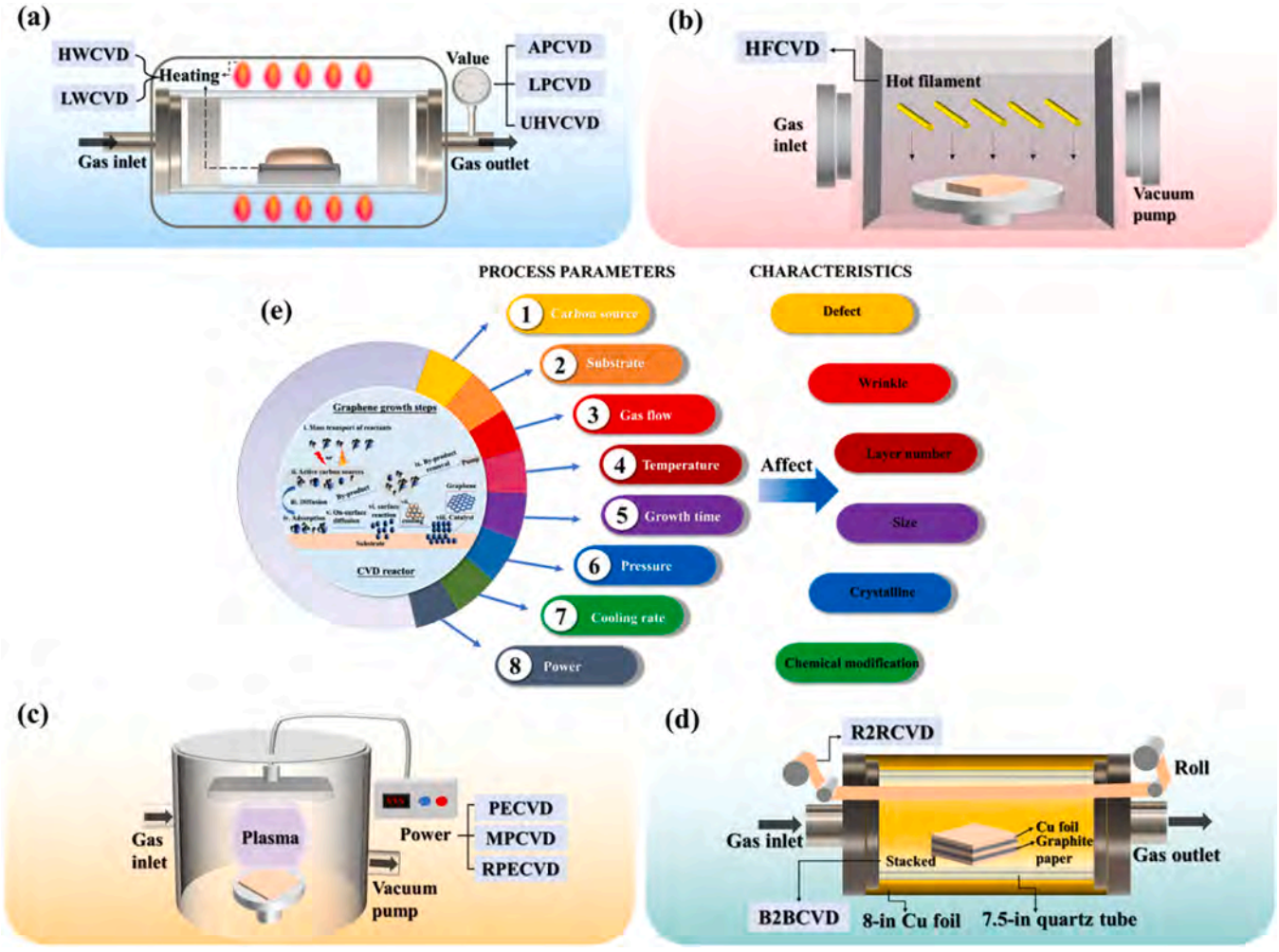

Fig. 5. Schematics of the diagram of equipment and growth process principles for large-scale production of CVD graphene. (a) Schematic diagrams of HWCVD, LWCVD, APCVD, LPCVD, and UHVCVD systems; (b) Schematic diagram of the HFCVD system; (c) Schematic diagrams of PECVD, MPCVD, and RPECVD systems; (d) Schematic diagrams of B2BCVD and R2RCVD systems. In the B2B process, Cu substrates are stacked to increase the production capacity, while in the R2R process, the Cu foil is moved continuously in the furnace; (e) Schematic diagram illustrating the growth steps, processing parameters, and characteristics of graphene in the CVD chamber.

hot filaments at a temperature up to 2000 ℃ to produce the carbon sources that diffuse and deposit on the substrate surface for graphene growth, and the substrate temperature varies with the filament distance and power [178,179]. Reducing the graphene growth energy consumption and enabling lower temperature synthesis on substrates with poor heat resistance are industrially desirable. Traditional thermal CVD is challenged at low temperatures due to high activation energies. Notably, plasma technology effectively enables low-temperature growth by substituting electron kinetics for heat [180]. Plasma methods include microwave plasma CVD (MPCVD), plasma-enhanced CVD (PECVD), and remote plasma-enhanced CVD (RPECVD), as shown in Fig. 5c [181]. By introducing active plasma species, PECVD lowers the reaction temperature, accelerates surface diffusion, and makes graphene synthesis on temperature-sensitive substrates possible [182]. Moreover, the in situ growth of high-quality graphene on temperature-sensitive industrial substrates poses a challenge in balancing growth temperature and quality [183]. Lowering the temperature while maintaining the quality requires continuous progress to overcome the technical hurdles, an important focus for further research.

Large-scale graphene production techniques have evolved from traditional hot CVD to lower-temperature PECVD, with the goal of enabling industrial-level batch manufacturing through roll-to-roll (R2R) and bench-to-bench (B2B) processes (Fig. 5d). These techniques aim to address the limitations of traditional quartz tube-based CVD in terms of size and uniformity. The B2B process stacks Cu foil layers separated by graphene sheets, significantly increasing the graphene yield per batch. Bae et al. have demonstrated a B2B system wrapped with quartz tubes of 7.5 in. in Cu foil and suspending it in a larger quartz tube of 8 in. to maximize the graphene film area and uniformity [184]. Xu et al. have used the B2B process by stacking Cu foils layer-by-layer and separating them with graphene paper to increase the graphene area per batch and scale up production by 20 folds [185]. By optimizing the metal foil thickness and spacing, ultra-large graphene films can be grown in relatively compact reactors. R2R is more suitable for continuous, high-throughput manufacturing and enables wafer-scale synthesis with yields over 30 times higher than that of conventional methods. Applications have been demonstrated in flexible electronics such as touch screens and OLEDs [186]. However, high temperature and plasma collaboration are still required to facilitate efficient, growth across long rolls. Researchers have adopted the MWCVD system at 400 ℃ with 8 linear antennas and a 2.45 GHz microwave generator for rapid, uniform heating of wide rolls [187]. Alternative joule heating-based R2R systems have also been proposed for rapid growth at 1000 ℃ through direct resistive heating of Cu [188]. Growing graphene directly on Cu poses challenges due to Cu softening at high temperatures. To address this, APCVD has been tested using roll-encapsulated Cu for in-situ heating, growth, and cooling. While this protected the Cu, growth remained non-uniform under the limitations of APCVD [189]. Recently, a concentric tube CVD R2R reactor has been designed with separate annealing and growth zones. In this system, the Cu substrate undergoes spiral polishing to promote highly uniform graphene synthesis [190]. In summary, both B2B and R2R enable large-area high-throughput graphene film growth.

While CVD allows for large-area production of high-quality graphene thin films, direct growth of graphene on large areas on various industrial substrates remains a challenge. The key issues are that most industrial substrates cannot withstand the high temperature required for conventional CVD growth. The B2B and R2R processes also depend on Cu foils as the intermediate transfer carrier. Direct in situ growth of graphene on wear-resistant component substrates like machine parts can eliminate complex transfer steps and avoid potential issues during transfer. This will help to fully realize the macroscale superlubricity properties in real applications. The goal of advancing CVD equipment and processes is to develop methods for direct, large-area deposition of high-quality graphene on any substrates.

5.2. CVD graphene growth thermodynamics, kinetics and factors

Thermodynamics and kinetics jointly govern graphene growth and features during CVD, as shown in Fig. 5e. Thermodynamics assesses the feasibility and directionality of the reaction by calculating the energies and stabilities and predicting the optimal conditions and pathways. Kinetics reveals growth rates and mechanisms from rate constants and pathways to provide timescale and steps. Integrated thermodynamics-kinetic analysis enhances our understanding of the optimal conditions, mechanisms, and rates in a more complete way crucial to the control of high-quality graphene production and applications.

5.2.1. Thermodynamic process in CVD graphene growth

Thermodynamic processes describe whether chemical reactions will occur under certain conditions. Hydrocarbons, such as methane (CH_4), ethanol (C_2H_5OH), acetylene (C_2H_2), and benzene (C_6H_6), are commonly used as carbon sources. However, breaking C-H bonds, which can require up to 414 kJ/mol of energy, typically occurs at high temperatures [173]. To lower the growth temperature, various catalysts are used to lower the activation energy barrier. Therefore, thermodynamic calculations can provide insights into the activation energy and relative stability of active carbon species during graphene synthesis. Recent studies have highlighted how different substrates and carbon precursors influence the growth temperature and energy consumption of the graphene growth process, as shown in Fig. 6a [191]. For instance, Liu et al. have found that graphene synthesis is more energy efficient on metal substrates compared to oxide or nitride substrates using the same carbon source [192]. Additionally, C_6H_6 and C_2H_2 decrease the required growth temperature [193]. Carbon precursors with inherently lower bond dissociation energies, such as ethane (C_2H_6), toluene (C_7H_8), and pyridine (C_5H_5N) have also been employed to lower the activation temperature [194,195]. Complementing these findings, Davies et al. have analyzed the thermochemical vapor-phase equilibrium and reported that CH_4 begins cracking at 250 ℃, leading to increased hydrogen concentrations in equilibrium at 450 ℃ [196]. Further decomposition occurs with increasing temperature until a minimum is reached at 1200 ℃. Moreover, C_6H_6 is present between 300–800 ℃, with C_2H_2 being the most stable active carbon source below 1000 ℃, followed by ethylene (C_2H_4) [197,198]. Ding et al. have calculated the binding energy (Eb) to evaluate the thermodynamic lifetime of active carbon species on metallic catalysts, as shown in Eq. (1) [199]:

$$E_b = E_M + E_{CH_i} - E_T \tag{1}$$

where E_M, E_{CH_i}, and E_T represent the binding energies on the metallic substrate, CH_i, and the given structure respectively. As shown in the graph, for different metallic substrates, with i increasing to 4, the binding energy of CH_4 is the lowest, indicating the weakest interaction between metal and methane molecules and the minimum activation energy required, suggesting that the thermal decomposition of CH_4 is relatively facile on metallic substrates. The interaction between C and metal can be calculated based on the width and energy of the *d*-orbitals of the metal to evaluate the thermodynamic lifetime of C on metallic substrates [200]. According to Eq. (2), both the temperature and binding energy determine the thermodynamic lifetime. Tighter binding carbon sources mean stronger interactions between carbon atoms and the metallic substrate, resulting in a longer thermodynamic lifetime at higher binding energies [199].

$$\tau = \tau_0 \exp\left(\frac{E_b}{k_B T}\right) \tag{2}$$

The Arrhenius Eq. (3) can be used to explain how lowering the activation energy leads to a lower activation temperature [176].

$$k = A e^{\frac{-E_a}{RT}} \tag{3}$$

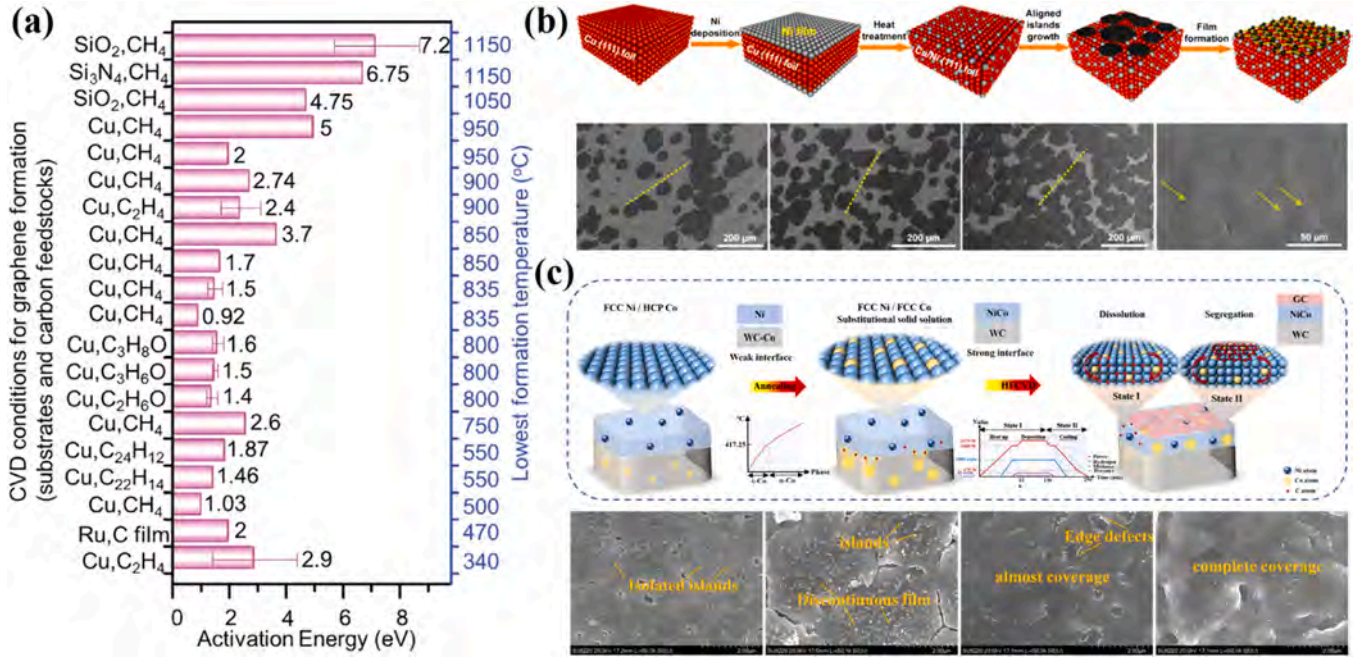

Fig. 6. (a) Activation energy for CVD graphene formation; (b) Schematic and coverage morphology of the single-layer graphene on Cu/Ni (111) alloy foils for 1 min, 2 min, 3 min, and 5 min, respectively; (c) Schematic and coverage morphology of the multi-layer graphene on NiCo alloy for 0 μm, 0.4 μm, 0.7 μm, and 1 μm solid solution depths. [191], copyright 2021, Wiley-VCH. [221], copyright 2018, ACS. [225], copyright 2024, Elsevier.
(a) Thermodynamic effects of the carbon source and substrate on graphene growth. (b) [(a) adapted with permission from Ref. (c) (b) adapted with permission from Ref. (d) (c) adapted with permission from Ref.

where k is the rate constant, R is the gas constant, T is the reaction temperature, E_a is the decomposition activation energy, A is the pre-exponential factor. and k bears an exponential relationship with E_a. When the activation energy decreases, the rate constant increases and the reaction rate accelerates. This means sufficient reactivity of active carbon species can still support graphene growth even at lower temperatures. The stability of active carbon species on the substrate can be determined by the relative Gibbs free energy (ΔG), as shown in Eq. (4) [199]:

$$\Delta G_f = E_T - E_M + \Delta F_{vib} - n_c\mu_c - n_H\mu_H \tag{4}$$

where ΔF_{vib} is the vibrational contribution to ΔG_f, n_c and n_H represent the numbers of carbon and hydrogen atoms in the substance, and μ_c and μ_H are the chemical potentials of carbon and hydrogen, respectively, which depend on the growth temperature and partial pressures of methane and hydrogen gas.

5.2.2. *CVD thermodynamic effects on structure and tribological properties of graphene*

The carbon sources and catalytic substrates play an important role in controlling the surface quality, uniformity, and layer numbers of graphene during the thermodynamic process of growth. Carbon sources can exist in solid, liquid, or gaseous states, each participating differently during synthesis. Solid carbon sources vaporize upon heating and enter the reaction zone carried by a carrier gas [201]. The rate of vaporization and resulting gaseous carbon concentration vary with the temperatures. For example, Wu et al. have used solid polystyrene as the carbon source to produce a single-crystal graphene coating on a Cu substrate using elevated temperature vaporization [202]. As the carbon source temperature increases, more carbon volatilizes, leading to a gradual rise in the layer number of graphene coatings. Liquid carbon sources are introduced by injection, with the concentration determined by the injection rate [194]. Common liquid carbon sources include C_2H_5OH, C_7H_8, and cyclohexane (C_6H_{12}). Lisi et al. have generated high-quality graphene coating with clean surfaces using Cu and C_2H_5OH [203]. Gaseous hydrocarbons, the most prevalent carbon sources, like CH_4, C_2H_2, propane (C_3H_8), and C_2H_4, enter directly [204]. Wassei et al. have examined the effects of these alkanes on layer formation and found that methane typically forms monolayers, ethane can yield single or bilayers, and propane produces uneven multilayers [205]. This indicates shorter-chain alkanes promote the growth of high-quality, uniform graphene coatings.

Catalytic substrates for graphene synthesis can be classified into two main categories: low-activity insulators and high-activity metals. Insulators such as SiO_2 [206], h-BN [207], and Al_2O_3 [208] are extensively researched for their capacity to support in-situ growth, eliminating the need for additional transfer during the fabrication of electronic device [209]. However, the growth of graphene on insulators faces significant challenges. The low catalytic activity results in slower growth rates and lower quality graphene compared to that deposited on metal catalysts [210]. To improve the nucleation and growth of high-quality graphene on insulators, researchers have adopted various strategies, including the introduction of catalytic gases [211], utilization of traditional external metal catalysts [212], and the application of electromagnetic induction heating systems [213]. Despite these advancements, the complexity of these methods continues to impede their macroscale application in the field of graphene solid lubricants. Metals such as Cu and Ni belong to the former due to their high catalytic ability, typically yielding graphene with superior quality [214]. For low carbon solubility metals like Cu, surface carbon is directly consumed by surface diffusion, where carbon species adsorb to form nucleation sites that grow into graphene by additional carbon accretion [215,216]. High solubility metals like Ni fully dehydrogenate active carbon into dissolved atomic carbon, which later precipitates during cooling to form graphene [217]. Thus, surface diffusion favors single/few layers while precipitation enables multilayers [218]. Kim et al. have deposited graphene on Cu and Ni metal catalysts using CVD and found that the multilayer graphene grown on Ni exhibited a lower COF and enhanced wear resistance compared to that grown on Cu [219]. In addition to single metal catalysts, alloyed substrates have been studied to synthesize graphene. As aforementioned, Cu

exhibits weaker catalytic activity and lower solubility than Ni, thus hindering multilayer growth with Cu alone. Leveraging the advantages of both, Cu-Ni alloys have been employed, with nickel promoting interface charge transfer and surface activity for uniform, high-quality graphene, as shown in Fig. 6b [220–223]. Zou et al. have employed CVD to grow high-quality and uniform graphene coatings on NiCu alloy, achieving lower COF and wear rates [224]. Additionally, Fan et al. have exploited the competitive catalytic reaction of NiCo alloys to deposit conformally encapsulated and high-coverage graphene coatings directly on hard substrates by HFCVD, as shown in Fig. 6c [225]. These coatings exhibit superior lubricity and durability in industrial applications. Alloying provides a means to modulate the interfacial interactions and optimize graphene synthesis by balancing various substrate characteristics. The other properties of the catalytic substrate, such as the thermal expansion coefficient and crystallinity, also influence the formation of graphene by impacting thermal and lattice mismatch during growth which in turn affects the distribution and density of surface defects [101, 226].

5.2.3. Kinetic process of CVD graphene growth

The key steps in CVD graphene growth kinetics include nucleation, growth, self-assembly, and agglomeration, influenced by substrate carbon solubility, catalytic activity, temperature, and gas pressure. The growth rate depends on the diffusion and consumption of active carbon species at the substrate surface, as shown by Eqs. (5) and (6) [175]:

$$F_{mass\ transport} = h_g(C_g - C_s) \tag{5}$$

$$F_{surface\ reaction} = k_s C_s \tag{6}$$

where $F_{mass\ transport}$ and $F_{surface\ reaction}$ denote the flux of active carbon species through the boundary layer and consumed in graphene growth, respectively. h_g is the mass transfer coefficient, k_s is the surface reaction constant, and C_g and C_s represent the concentration of active carbon species in the gas phase and substrate surface, respectively. Generally, the CVD system pressure determines the boundary layer thickness and carbon collisions and diffusion rates, thereby affecting the mass transport rate. The substrate properties like catalytic ability and carbon solubility, determined by unoccupied d-orbitals, also influence the surface reaction rates. For instance, Cu lacks unoccupied d orbitals and has low carbon solubility thus exhibiting weaker catalytic ability [227]. Conversely, Ni, with strong interaction between its *d* orbitals and carbon's *p* orbitals along with higher carbon solubility, shows higher the surface reaction rates [228]. During nucleation, classical nucleation theory is shown in the following:

$$N = AP(T)\exp(\frac{E_{des} - E_s - \Delta G^*}{kT}) \tag{7}$$

where N represents the nucleation rate, A is a constant, k stands for the Boltzmann constant, T signifies temperature, P denotes the pressure, E_{des} is the energy of surface desorption, E_s is the activation energy for surface diffusion, and ΔG^* is free energy. The classical nucleation theory shows that the nucleation rate (N) depends on factors such as temperature, pressure, and substrate interactions based on the equations involving constants, the Boltzmann factor, and free energy [229,230]. After nucleation, epitaxial growth occurs as carbon species diffuse and attach to graphene edges, consequently slowing with expanding area due to limited species/diffusion [231]. Eventually, the rates of growth and etching reach a dynamic equilibrium. The coverage area of graphene on the substrate is determined by the temperature-dependent equilibrium constants and the partial pressure of the carbon source and hydrogen gas, as shown in the following equation [232]:

$$A_G = 1 - \frac{P_{H_2}}{K_1 K_2 K_3 \rho_S P_{CH_4}} \tag{8}$$

where K_1, K_2, and K_3 are the adsorption and desorption equilibrium constants of CH_4, H_2, and carbon species at the graphene edge. Finally, the self-assembly and agglomeration process, influenced by substrate crystal orientation, grain boundaries, and size, determines the quality and performance of graphene growth [233–235].

5.2.4. CVD kinetic effects on structure and tribological properties of graphene

The kinetics parameters, such as working pressure, temperature, time, gas flow ratios, and cooling rate influence the properties and structure of CVD graphene. Bhaviripudi et al. have observed significant variations in formation even at constant thermodynamics in different environments [175]. Specifically, LPCVD shows 95 % monolayer coverage versus APCVD due to excess carbon precursors from a high pressure, leading to the growth of few-layer hexagonal structures with AB Bernal stacking [236]. The ratio of the precursor gases also impacts the surface concentration of carbon species on the metal catalyst, and consequently the quality of the resultant graphene. Son et al. have synthesized high-quality graphene at a low total pressure with optimized CH_4:H_2 ratios [237]. In another study, the films morph from irregular nanosheets to a uniform hexagonal morphology when the ratio is changed to 1:12.5 (Fig. 7a) [238]. Tripathi et al. have adjusted CH_4 flow rates from 50 to 200 sccm in CVD to deposit graphene on gray cast iron and found that the lowest flow rate produced the most uniform graphene with superior friction performance [239]. Moreover, Shen et al. have found that reducing working pressure from 4000 Pa to 600 Pa in CVD increased the number of graphene layers, with bilayer graphene showing optimal lubricity and wear resistance [178].

Hydrogen is often used in CVD growth of graphene to serve the dual roles of a surface activator and etchant. As an activator, H_2 stimulates carbon source activation and growth through reactions on the catalyst surface [240]. Specifically, H_2 decomposes into active H atoms on the Ni catalyst surface, triggers CH_4 decomposition into reactive CH_3, (CH_2)s, and (CH)s radicals, and drives graphene formation [241]. Moreover, hydrogen acts as an etchant and moderates the grain size and morphology of graphene [242]. Owing to graphene's structural irregularity, hydrogen selectively etches weak C-C bonds to aid the production of uniform and fine grains [243]. A suitable hydrogen amount can also diminish the defect density and improve the crystal quality [244]. However, excessive H_2 flow may lead to increased roughness and wrinkling of graphene [245]. Hydrogenated graphene coatings grown at moderate hydrogen flow rates (1000 sccm) exhibit excellent surface quality ($0 < I_D/I_G < 0.21$) and smoothness, thus maximizing the benefits of macroscale superlubricity, as shown in Fig. 7b [102].

CVD synthesis of graphene typically requires a high temperature (~1000 ℃), potentially inducing thermal shrinkage of the cooling substrate and consequent graphene wrinkling [246]. Therefore, judicious control of the growth temperature and time is pivotal. The optimal growth temperature for graphene varies with the catalyst substrate: > 800 ℃ for Ni, 850–1000 ℃ for Co/Fe, and 900–1050 ℃ for Cu [173]. A higher temperature (>1035 ℃) fosters the formation of low-density graphene nuclei and larger grains, but rougher surfaces from metal evaporation [247]. Conversely, lower temperature (<800 ℃) produces a transition in graphene grains from hexagonal to dendritic structures and amorphous carbon films [248]. The carbon sources also influence the growth temperature. Sun et al. have synthesized large-area single--crystal graphene using ethane as a carbon precursor instead of methane and found that graphene growth requires > 900 ℃ with methane, but only 750 ℃ with C_2H_6 [249]. Li et al. have employed PMMA, polystyrene or C_6H_6 as the carbon sources to synthesize graphene by thermal decomposition in the temperature range of 800–980 ℃, as shown in Fig. 7c [194]. Moreover, these carbon sources allow for the growth of centimeter-scale monolayer graphene films at a temperature as low as 400 ℃. The growth time and temperature are also crucial to graphene growth. Singh et al. have investigated the impact of growth temperature, C_2H_2 flow rate, and reaction time on graphene synthesis using CVD and found that optimal conditions—850 ℃, 6 sccm C_2H_2, and

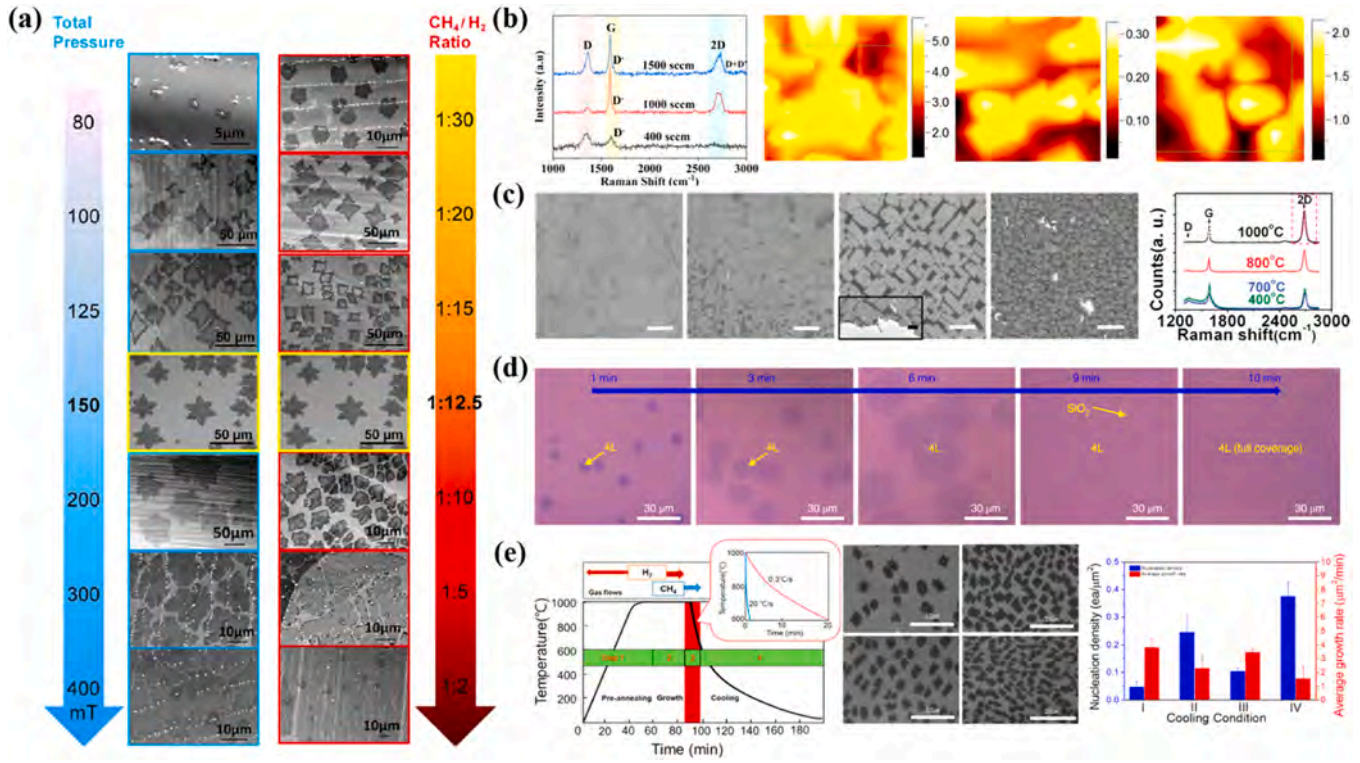

Fig. 7. Kinetic effect on CVD graphene growth. (a) Graphene morphologies using various pressure and CH_4/H_2 ratio; (b) Raman spectra and mapping of graphene grown at 400 sccm, 1000 sccm, and 1500 sccm hydrogen flow rates; (c) Graphene morphologies and Raman spectra of sample grown at 1000 ℃, 800 ℃, 700 ℃, and 400 ℃; (d) Graphene morphologies and layers number evolution with time; (e) Graphene morphologies and nucleation site density under different cooling conditions. [238], copyright 2012, ACS. [102], copyright 2023, Elsevier. [194], copyright 2011, ACS. [252], copyright 2020, Springer Nature. [259], copyright 2014, ACS].
(a) [(a) adapted with permission from Ref. (b) (b) adapted with permission from Ref. (c) (c) adapted with permission from Ref. (d) (d) adapted with permission from Ref. (e) (e) adapted with permission from Ref.

10 min—yielded high-quality graphene with reduced friction and wear rates [250]. Longer time enlarges the graphene grains without altering the thickness on Cu, but on Ni, it increases the amount of dissolved carbon into the substrate and adds the number of graphene layers. Boyd et al. have found reduced defects and high-quality single-crystal graphene with extended Cu growth time [180]. Similarly, Park et al. have observed improved quality, larger grains, and formation of large-area graphene films by reducing the growth temperature and extending the growth time [251]. Nguyen et al. have shown that time enables island merging into continuous monolayer graphene films on the Cu-Si alloy substrate, as shown in Fig. 7d [252]. Moreover, Won et al. have deposited graphene on Cu substrates using CVD and found that extending growth time from 5 to 20 min significantly improved the coating's uniformity and quality, thereby enhancing wear resistance [253]. The cooling rates modulate the graphene quality by governing carbon diffusion and segregation during CVD growth kinetics. The mechanisms differ between Ni and Cu substrates. Graphene formation relies more on carbon segregation/deposition on Ni but surface nucleation sites on Cu, implying that cooling rate alterations impact the nucleation density, growth rate, and layer number of graphene [254, 255]. A faster cooling rate curbs carbon segregation in high-solubility metals like Ni, favoring high-quality monolayer and bilayer graphene [256]. For example, during thin Ni layer deposition on SiO_2/Si substrate, rapid cooling can decrease carbon diffusion to suppress multilayer graphene formation [257]. As the carbon concentration drops from the metal surface to the substrate, a faster cooling rate produces quenching effects to slow carbon migration to the metal surface and reduce the nucleation density [258]. Conversely, slower cooling provides time for carbon permeation into the substrate and elevates the nucleation density as shown in Fig. 7e [259]. By compromising the crystallinity, this enhances multilayer formation. Under optimal moderate conditions, high-quality multilayers can be synthesized by balancing these effects.

In summary, the thermodynamics and kinetics in CVD graphene growth render the process complex with multiple steps. Comprehending these critical stages and influencing factors allows for better control and optimization of CVD graphene deposition. This enables the fabrication of large-scale, high-quality coatings of graphene on various substrates for applications requiring superlubricity.

6. Conclusions and outlooks

Graphene solid lubricants with superlubricity properties remain at the conceptual and micro/nanoscopic design stage as evidenced by extensive simulations and experiments. Current research efforts have focused on elucidating the macroscale superlubricity mechanisms including the incommensurate structures, chemical interactions, and microstructural effects. While macroscale experiments demonstrate the feasibility, bridging the scaling gap between micro/nanoscale and macroscale superlubricity mechanisms necessitates further investigation. Closing this gap between scales would help in developing graphene coatings for macroscale applications. Additionally, the service life of graphene solid lubricants is a major factor limiting engineering applications. It is necessary to figure out how to maintain stable friction reduction or superlubricity under harsh conditions. CVD techniques have been improved for the large-scale fabrication of graphene coatings, but the in situ growth of large-area, high-quality, and uniform graphene coatings on industrial substrates remains a challenge. To facilitate the large-scale engineering application of superlubricity in graphene solid lubricant, several issues must be addressed through promising avenues.

(1) High-quality, large-area, and uniform graphene solid lubricants with weakened interfacial interactions are key to macroscale superlubricity. Optimizing the CVD processes and assessing B2B and R2R approaches are important to ensure scalable graphene deposition. However, in situ graphene growth on industrial substrates remains challenging.
(2) Graphene superlubricity follows the basic mechanism of interlayer weak interactions during sliding at the interfaces, but the mechanism of macroscale superlubricity may not be universally applicable on the micro/nanoscale. Combining graphene with nanoparticles or dividing substrate surfaces into numerous microcontact regions may be effective strategies to obtain cross-scale superlubricity.
(3) Under harsh conditions, the bond strength between the graphene coating and the substrate is critical for the durability and reliability. Further research elucidating the superlubricity performance and mechanisms of graphene under high temperature, high speed, high load, high vacuum, inert gases, electric fields, and magnetic fields are needed for the industrial application of graphene solid lubricants under harsh conditions.
(4) Extending the macroscale graphene superlubricity lifetime is crucial. Covalent or non-covalent modification of graphene surfaces with nanoparticles or heterogeneous 2D materials, as well as the introduction of high-bearing phases, are important research areas for effective increase of the macroscale superlubricity lifetime of graphene.
(5) Exploring how natural organisms achieve ultra-low friction by modifying surface structures may offer valuable insights into mechanisms of superlubricity, facilitating the development of innovative biomimetic designs in lubrication filed.
(6) Integrating sensors and microprocessors to dynamically monitor and adjust the structural and properties of graphene under various conditions may enable the development of intelligent lubrication systems.
(7) Exploring the integration of multifunctional features such as corrosion resistance, thermal stability, and electromagnetic shielding into graphene solid lubricant may enhance their versatility and appeal for diverse industrial applications.

Although graphene coatings for industrial solid lubrication are still being developed, the worldwide need for energy and precise equipment provides a favorable environment. Graphene solid lubricants are expected to overcome the limitations and transition from the laboratory to market applications in the future.

CRediT authorship contribution statement

Jing Wu: Validation, Investigation, Data curation. **Guohua Chen:** Validation, Supervision. **Shu Xiao:** Writing – review & editing, Supervision, Resources, Project administration, Funding acquisition. **Paul K. Chu:** Writing – review & editing, Supervision, Resources, Project administration, Funding acquisition. **Yinong Chen:** Writing – original draft, Investigation, Data curation, Conceptualization. **Fan shuyu:** Writing – review & editing, Writing – original draft, Investigation, Data curation, Conceptualization.

Declaration of Competing Interest

The authors declare that they have no known competing financial interests or personal relationships that could have appeared to influence the work reported in this paper.

Data availability

Data will be made available on request.

Acknowledgments

This work is supported by the National Natural Science Foundation of China (No. 52375182 and 52005187), Natural Science Foundation of Guangdong Province (No.2023A1515012308), Fundamental Research Funds for the Central Universities (No.2023ZYGXZR030), Basic and Applied Basic Research Foundation of Guangzhou (No.2024A04J3821), as well as City University of Hong Kong Strategic Research Grant (SRG No. 7005505).

References

[1] Woon KS, Phuang ZX, Taler J, Varbanov PS, Chong CT, Klemes JJ, Lee CT. Recent advances in urban green energy development towards carbon emissions neutrality. Energy 2023;267:126502.
[2] Rejith R, Kesavan D, Chakravarthy P, Murty SVSN. Bearings for aerospace applications. Tribol Int 2023;181:108312.
[3] Ernesto CN, Mario TP, Juan CJC, Roberto VCS, José GRM. Expert control systems for maximum power point tracking in a wind turbine with PMSG: State of the art. Appl Sci 2019;9(12):2469.
[4] Bhadeshia HKDH. Steels for bearings. Prog Mater Sci 2012;57(2):268–435.
[5] Li RY, Sun CJ, Yang X, Wang YF, Gao KX, Zhang JY, Li JG. Toward high load-bearing, ambient robust and macroscale structural superlubricity through contact stress dispersion. Chem Eng J 2022;431:133548.
[6] Page F, Poll G. Investigations on graphene platelets as dry lubricant and as grease additive for sliding contacts and rolling bearing application. Lubricants 2020;8(3):1–12.
[7] Wang XB, Zhang YF, Yin ZW. Frequent start-stop test study of graphene coatings on journal bearings. Key Eng Mater 2020;841:26–35.
[8] Holmberg K, Erdemir A. Influence of tribology on global energy consumption, costs and emissions. Friction 2017;5(3):263–84.
[9] Berman D, Erdemir A, Sumant AV. Graphene: a new emerging lubricant. Mater Today 2013;17(1):31–42.
[10] John M, Menezes PL. Self-lubricating materials for extreme condition applications. Materials 2021;14(19):5588.
[11] Liu JL, Zhang YY, Liao B. A review on preparation process and tribological performance of coatings for internal combustion engine piston ring. Adv Mech Eng 2023;15(5):16878132231175752.
[12] Lee CG, Wei XD, Kysar JW, Hone J. Measurement of the elastic properties and intrinsic strength of monolayer graphene. Science 2008;321(5887):385–8.
[13] Li SZ, Li QY, Carpick RW, Gumbsch P, Liu XZ, Ding XD, Sun J, Li J. The evolving quality of frictional contact with graphene. Nature 2016;539(7630):541–5.
[14] Balandin AA. Thermal properties of graphene and nanostructured carbon material. Nat Mater 2011;10(8):569–81.
[15] Berry V. Impermeability of graphene and its applications. Carbon 2013;62:1–10.
[16] Zhai WZ, Zhou K. Nanomaterials in superlubricity. Adv Funct Mater 2019;29(28):1806395.
[17] Song YM, Qu CY, Ma M, Zheng QS. Structural superlubricity based on crystalline materials. Small 2020;16(15):1903018.
[18] Wang J, Cao W, Song YM, Qu CY, Zheng QS, Ma M. Generalized scaling law of structural superlubricity. Nano Lett 2019;19(11):7735–41.
[19] Zhang DL, Li ZB, Klausen LH, Li Q, Dong MD. Friction behaviors of two-dimensional materials at the nanoscale. Mater Today Phys 2022;27:100771.
[20] Ge XY, Chai ZY, Shi QY, Liu YF, Wang WZ. Graphene superlubricity: a review. Friction 2023;11(11):1953–73.
[21] Marian M, Berman D, Rota A, Jackson RL, Rosenkranz A. Layered 2D nanomaterials to tailor friction and wear in machine elements—a review. Adv Mater Interfaces 2022;9(3):2101622.
[22] Ramezani M, Ripin ZM, Jiang CP, Pasang T. Superlubricity of materials: progress, potential, and challenges. Materials 2023;16(14):5145.
[23] Wu FB, Zhou SJ, Ouyang JH, Wang SQ, Chen L. Structural superlubricity of two-dimensional materials: mechanisms, properties, influencing factors, and applications. Lubricants 2024;12(4):138.
[24] Ge XY, Chai ZY, Shi QY, Liu YF, Wang WZ. Graphene superlubricity: a review. Friction 2023;11(11):1953–73.
[25] Bao J, Chen GY, He YY, Zhang CH, Luo JB. Lubrication properties of graphene under harsh working conditions. Mater Today Adv 2023;18:100369.
[26] Liu YF, Ge XY, Li JJ. Graphene lubrication. Appl Mater Today 2020;20:100662.
[27] Liu LC, Zhou M, Jin L, Li LC, Mo YT, Su GS, Li X, Zhu HW, Tian Y. Recent advances in friction and lubrication of graphene and other 2D materials: mechanisms and applications. Friction 2019;7(3):199–216.
[28] Berman D, Erdemir A, Sumant AV. Approaches for achieving superlubricity in two-dimensional materials. ACS Nano 2018;12(3):2122–37.
[29] Jia KC, Zhang JC, Zhu YS, Sun LZ, Lin L, Liu ZF. Toward the commercialization of chemical vapor deposition graphene films. Appl Phys Rev 2021;8(4):041306.
[30] Wang LY, Lai RZ, Zhang LC, Zeng MQ, Fu L. In situ investigating the mechanism of graphene growth by chemical vapor deposition. ACS Mater Lett 2022;4(4):528–40.
[31] Peyrard M, Aubry S. Critical behaviour at the transition by breaking of analyticity in the discrete Frenkel-Kontorova model. J Phys C 1983;16:1593–608.
[32] Hirano M, Shinjo K. Atomistic locking and friction. Phys Rev B 1990;41(17):11837–51.

[33] Zhang RF, Ning ZY, Zhang YY, Zheng QS, Chen Q, Xie HH, Zhang Q, Qian WZ, Wei F. Superlubricity in centimeters-long double-walled carbon nanotubes under ambient conditions. Nat Nanotechnol 2013;8(12):912–6.
[34] Liu Z, Yang JR, Grey F, Liu JZ, Liu YL, Wang YB, Yang YL, Cheng Y, Zheng QS. Observation of microscale superlubricity in graphite. Phys Rev Lett 2012;108 (20):205503.
[35] Dienwiebel M, Verhoeven GS, Pradeep N, Frenken JWM, Heimberg JA, Zandbergen HW. Superlubricity of graphite. Phys Rev Lett 2004;92(12):126101.
[36] Li H, Wang JH, Gao S, Chen Q, Peng LM, Liu KH, Wei XL. Superlubricity between MoS_2 Monolayers. Adv Mater 2017;29(27):1701474.
[37] Song YM, Mandelli D, Hod O, Urbakh M, Ma M, Zheng QS. Robust microscale superlubricity in graphite/hexagonal boron nitride layered heterojunctions. Nat Mater 2018;17(10):894–9.
[38] Wang LF, Zhou X, Ma TB, Liu DM, Gao L, Li X, Zhang J, Hu YZ, Wang H, Dai YD, Luo JB. Superlubricity of a graphene/MoS_2 heterostructure: a combined experimental and DFT study. Nanoscale 2017;9(30):10846–53.
[39] Sharp TA, Pastewka L, Robbins MO. Elasticity limits structural superlubricity in large contacts. Phys Rev B 2016;93(12):121402.
[40] Berman D, Deshmukh SA, Sankaranarayanan SKRS, Erdemir A, Sumant AV. Macroscale superlubricity enabled by graphene nanoscroll formation. Science 2015;348(6239):1118–22.
[41] Liu SW, Wang HP, Xu Q, Ma TB, Yu G, Zhang CH, Geng DC, Yu ZW, Zhang SG, Wang WZ, Hu YZ, Wang H, Luo JB. Robust microscale superlubricity under high contact pressure enabled by graphene-coated microsphere. Nat Commun 2017;8: 14029.
[42] Li PP, Ju PF, Ji L, Li HX, Liu XH, Chen L, Zhou HD, Chen JM. Toward robust macroscale superlubricity on engineering steel substrate. Adv Mater 2020;32(36): 2002039.
[43] Hod O, Meyer E, Zheng QS, Urbakh M. Structural superlubricity and ultralow friction across the length scales. Nature 2018;563(7732):485–92.
[44] Stoyanov P, Chromik RR. Scaling effects on materials tribology: from macro to micro scale. Materials 2017;10(5):550.
[45] Olatomiwa AL, Adam T, Gopinath SCB, Kolawole SY, Olayinka OH, Hashim U. Graphene synthesis, fabrication, characterization based on bottom-up and top-down approaches: an overview. J Semicond 2022;43(6):061101.
[46] Choi SH, Yun SJ, Won YS, Oh CS, Kim SM, Kim KK, Lee YH. Large-scale synthesis of graphene and other 2D materials towards industrialization. Nat Commun 2022; 13(1):1484.
[47] Ullah S, Yang XQ, Ta HQ, Hasan M, Bachmatiuk A, Tokarska K, Trzebicka B, Fu L, Rummeli MH. Graphene transfer methods: a review. Nano Res 2021;14(11): 3756–72.
[48] Bahri M, Gebre SH, Elaguech MA, Dajan FT, Sendeku MG, Tlili C, Wang DQ. Recent advances in chemical vapor deposition techniques for graphene-based nanoarchitectures: from synthesis to contemporary applications. Coord Chem Rev 2023;475:214910.
[49] Lin L, Deng B, Sun JY, Peng HL, Liu ZF. Bridging the gap between reality and ideal in chemical vapor deposition growth of graphene. Chem Rev 2018;118(18): 9281–343.
[50] Shubha B, Praveen BM, Bhat V. Graphene - calculation of specific surface area. Int J Appl Eng Manag Lett 2023;7(1):91–7.
[51] Banhart F, Kotakoski J, Krasheninnikov AV. Structural defects in graphene. ACS Nano 2011;5(1):26–41.
[52] Tucek J, Blonski P, Ugolotti J, Swain AK, Enoki T, Zboril R. Emerging chemical strategies for imprinting magnetism in graphene and related 2D materials for spintronic and biomedical applications. Chem Soc Rev 2018;47(11):3899–990.
[53] Anwar A, Chang TP, Chen CT. Graphene oxide synthesis using a top-down approach and discrete characterization techniques: a holistic review. Carbon Lett 2022;32(1):1–38.
[54] Liao L, Peng HL, Liu ZF. Chemistry makes graphene beyond graphene. J Am Chem Soc 2014;136(35):12194–200.
[55] Niyogi S, Bekyarova E, Itkis ME, McWilliams JL, Hamon MA, Haddon RC. Solution properties of graphite and graphene. J Am Chem Soc 2006;128(24): 7720–1.
[56] Kurian M. Recent progress in the chemical reduction of graphene oxide by green reductants–A Mini review. Carbon Trends 2021;5:100120.
[57] Wu JB, Lin ML, Cong X, Liu HN, Tan PH. Raman spectroscopy of graphene-based materials and its applications in related devices. Chem Soc Rev 2018;47(5): 1822–73.
[58] Morrow WK, Pearton SJ, Ren F. Review of graphene as a solid state diffusion barrier. Small 2016;12(1):120–34.
[59] Munir KS, Wen C, Li YC. Carbon nanotubes and graphene as nanoreinforcements in metallic biomaterials: a review. Adv Biosyst 2019;3(3):1800212.
[60] Tsetseris L, Pantelides ST. Graphene: an impermeable or selectively permeable membrane for atomic species? Carbon 2014;67:58–63.
[61] Miao M, Nardelli MB, Wang Q, Liu YC. First principles study of the permeability of graphene to hydrogen atoms. Phys Chem Chem Phys 2013;15(38):16132–7.
[62] Bhatt MD, Kim H, Kim G. Various defects in graphene: a review. RSC Adv 2022;12 (33):21520–47.
[63] Zhan J, Lei ZD, Zhang Y. Non-covalent interactions of graphene surface: mechanisms and applications. Chem 2022;8(4):947–79.
[64] Balandin AA, Ghosh S, Bao WZ, Calizo I, Teweldebrhan D, Miao F, Lau CN. Superior thermal conductivity of single-layer graphene. Nano Lett 2008;8(3): 902–7.
[65] Ghosh S, Bao WZ, Nika DL, Subrina S, Pokatilov EP, Lau CN, Balandin AA. Dimensional crossover of thermal transport in few-layer graphene. Nat Mater 2010;9(7):555–8.
[66] Ghosh S, Calizo I, Teweldebrhan D, Pokatilov EP, Nika DL, Balandin AA, Bao W, Miao F, Lau CN. Extremely high thermal conductivity of graphene: prospects for thermal management applications in nanoelectronic circuits. Appl Phys Lett 2008;92(15):151911.
[67] Malekpour H, Ramnani P, Srinivasan S, Balasubramanian G, Nika DL, Mulchandani A, Lake RK, Balandin AA. Thermal conductivity of graphene with defects induced by electron beam irradiation. Nanoscale 2016;8(30):14608–16.
[68] Xu Y, Chen XB, Gu BL, Duan WH. Intrinsic anisotropy of thermal conductance in graphene nanoribbons. Appl Phys Lett 2009;95(23):233116.
[69] Guo ZX, Zhang D, Gong XG. Thermal conductivity of graphene nanoribbons. Appl Phys Lett 2009;95(16):163103.
[70] Evans WJ, Hu L, Keblinski P. Thermal conductivity of graphene ribbons from equilibrium molecular dynamics: effect of ribbon width, edge roughness, and hydrogen termination. Appl Phys Lett 2010;96(20):203112.
[71] Serov AY, Ong ZY, Pop E. Effect of grain boundaries on thermal transport in graphene. Appl Phys Lett 2013;102(3):033104.
[72] Zandiatashbar A, Lee GH, An SJ, Lee S, Mathew N, Terrones M, Hayashi T, Picu CR, Hone J, Koratkar N. Effect of defects on the intrinsic strength and stiffness of graphene. Nat Commun 2014;5:3186.
[73] López-Polín G, Gómez-Navarro C, Parente V, Guinea F, Katsnelson MI, Pérez-Murano F, Gómez-Herrero J. Increasing the elastic modulus of graphene by controlled defect creation. Nat Phys 2015;11(1):26–31.
[74] Tapia A, Peón-Escalante R, Villanueva C, Aviles F. Influence of vacancies on the elastic properties of a graphene sheet. Comput Mater Sci 2012;55:255–62.
[75] Xiao JR, Staniszewski J, Gillespie JW. Tensile behaviors of graphene sheets and carbon nanotubes with multiple Stone-Wales defects. Mater Sci Eng A 2010;527 (3):715–23.
[76] Dettori R, Cadelano E, Colombo L. Elastic fields and moduli in defected graphene. J Phys Condens Matter 2012;24(10):104020.
[77] Wang MC, Yan C, Ma L, Hu N, Chen MW. Effect of defects on fracture strength of graphene sheets. Comput Mater Sci 2012;54:236–9.
[78] Chen MQ, Quek SS, Sha ZD, Chiu CH, Pei QX, Zhang YW. Effects of grain size, temperature and strain rate on the mechanical properties of polycrystalline graphene - A molecular dynamics study. Carbon 2015;85:135–46.
[79] Yi LJ, Yin ZN, Zhang YY, Chang TC. A theoretical evaluation of the temperature and strain-rate dependent fracture strength of tilt grain boundaries in graphene. Carbon 2013;51:373–80.
[80] Rasool HI, Ophus C, Klug WS, Zettl A, Gimzewski JK. Measurement of the intrinsic strength of crystalline and polycrystalline graphene. Nat Commun 2013; 4:2811.
[81] Zhang JF, Zhao JJ, Lu JP. Intrinsic strength and failure behaviors of graphene grain boundaries. ACS Nano 2012;6(3):2704–11.
[82] Acik M, Chabal YJ. Nature of graphene edges: a review. Jpn J Appl Phys 2011;50 (7):070101.
[83] Batzill M. The surface science of graphene: metal interfaces, CVD synthesis, nanoribbons, chemical modifications, and defects. Surf Sci Rep 2012;67(3-4): 83–115.
[84] Kong LM, Enders A, Rahman TS, Dowben PA. Molecular adsorption on graphene. J Phys: Condens Matter 2014;26(44):443001.
[85] Yang G, Li LH, Lee WB, Ng MC. Structure of graphene and its disorders: a review. Sci Technol Adv Mater 2018;19(1):613–48.
[86] Cretu O, Krasheninnikov AV, Rodríguez-Manzo JA, Sun LT, Nieminen RM, Banhart F. Migration and localization of metal atoms on strained graphene. Phys Rev Lett 2010;105(19):196102.
[87] Wang Y, Shao YY, Matson DW, Li JH, Lin YH. Nitrogen-doped graphene and its application in electrochemical biosensing. ACS Nano 2010;4(4):1790–8.
[88] Boukhvalov DW, Katsnelson MI. Enhancement of chemical activity in corrugated graphene. J Phys Chem C 2009;113(32):14176–8.
[89] Parobek D, Liu HT. Wettability of graphene. 2D Mater 2015;2(3):032001.
[90] Zang JF, Ryu S, Pugno N, Wang QM, Tu Q, Buehler MJ, Zhao XH. Multifunctionality and control of the crumpling and unfolding of large-area graphene. Nat Mater 2013;12(4):321–5.
[91] Zhao GK, Li XM, Huang MR, Zhen Z, Zhong YJ, Chen Q, Zhao XL, He YJ, Hu RR, Yang TT, Zhang RJ, Li CL, Kong J, Xu JB, Ruoff RS, Zhu HW. The physics and chemistry of graphene-on-surfaces. Chem Soc Rev 2017;46(15):4417–49.
[92] Wang XL, Shi GQ. An introduction to the chemistry of graphene. Phys Chem Chem Phys 2015;17(43):28484–504.
[93] Spear JC, Custer JP, Batteas JD. The influence of nanoscale roughness and substrate chemistry on the frictional properties of single and few layer graphene. Nanoscale 2015;7(22):10021–9.
[94] Li QY, Liu XZ, Kim SP, Shenoy VB, Sheehan PE, Robinson JT, Carpick RW. Fluorination of graphene enhances friction due to increased corrugation. Nano Lett 2014;14:5212–7.
[95] Zeng XZ, Peng YT, Yu M, Lang HJ, Cao X, Zou K. Dynamic sliding enhancement on the friction and adhesion of graphene, graphene Oxide, and fluorinated graphene. ACS Appl Mater Interfaces 2018;10:8214–24.
[96] Ko JH, Kwon SK, Byun IS, Choi JK, Park BH, Kim YH, Park JY. dynamic sliding enhancement on the friction and adhesion of graphene, graphene oxide, and fluorinated graphene. Tribol Lett 2013;50:137–44.
[97] Shih CJ, Strano MS, Blankschtein D. Wetting translucency of graphene. Nat Mater 2013;12(10):866–9.
[98] Rafiee J, Mi X, Gullapalli H, Thomas AV, Yavari F, Shi YF, Ajayan PM, Koratkar NA. Wetting transparency of graphene. Nat Mater 2012;11(3):217–22.
[99] Liu YF, Ge XY, Li JJ. Graphene lubrication. Appl Mater Today 2020;20:100662.

[100] Li JH, Peng Y, Tang XQ, Liu B, Bai LC, Zhou K. Hydrogen-passivation modulation on the friction behavior of graphene with vacancy defects under strain engineering. Appl Surf Sci 2022;579:152055.
[101] Berman D, Deshmukh SA, Sankaranarayanan SKRS, Erdemir A, Sumant AV. Extraordinary macroscale wear resistance of one atom thick graphene layer. Adv Funct Mater 2014;24(42):2978–84.
[102] Fan SY, Xiao S, Lin SS, Su FH, Su YF, Chu PK. Macroscale superlubricity and durability of in situ grown hydrogenated graphene coatings. Chem Eng J 2023;459:141521.
[103] Chouhan A, Mungse HP, Khatri OP. Surface chemistry of graphene and graphene oxide: a versatile route for their dispersion and tribological applications. Adv Colloid Interface Sci 2020;283:102215.
[104] Wang Y, Qin J, Xu JX, Sun JH, Chen L, Qian LM, Kubo M. Definition of atomic-scale contact: what dominates the atomic-scale friction behaviors? Langmuir 2022;38(38):11699–706.
[105] Li PP, Wang B, Ji L, Li HX, Chen L, Liu XH, Zhou HD, Chen JM. Environmental molecular effect on the macroscale friction behaviors of graphene. Front Chem 2021;9:679417.
[106] Xiao YC, Shi XL, Zhai WZ, Kang Y, Yao J. Effect of temperature on tribological properties and wear mechanisms of NiAl matrix self-lubricating composites containing graphene nanoplatelets. Tribol Trans 2015;58(4):729–35.
[107] Liu YF, Li JJ, Ge XY, Yi S, Wang HD, Liu YH, Luo JB. Macroscale superlubricity achieved on the hydrophobic graphene coating with glycerol. ACS Appl Mater Interfaces 2020;12(16):18859–69.
[108] Dwivedi N, Patra T, Lee JB, Yeo RJ, Srinivasan S, Dutta T, Sasikumar K, Dhand C, Tripathy S, Saifullah MSM, Danner A, Hashmi SAR, Srivastava AK, Ahn JH, Sankaranarayanan SKRS, Yang H, Bhatia CS. Slippery and wear-resistant surfaces enabled by interface engineered graphene. Nano Lett 2020;20(2):905–17.
[109] Jia Q, Yang Z, Zhang B, Gao K, Sun L, Zhang J. Macro superlubricity of two-dimensional disulphide/amorphous carbon heterogeneous via tribochemistry. Mater Today Nano 2023;21:100286.
[110] Liao MZ, Nicolini P, Du LJ, Yuan JH, Wang SP, Yu H, Tang J, Cheng P, Watanabe K, Taniguchi T, Gu L, Claerbout VEP, Silva A, Kramer D, Polcar T, Yang R, Shi DX, Zhang GY. UItra-low friction and edge-pinning effect in large-lattice-mismatch van der Waals heterostructures. Nat Mater 2022;21(1):47–53.
[111] Müser MH. Structural lubricity: role of dimension and symmetry. Europhys Lett 2004;66(1):97–103.
[112] Urbakh M. Friction: towards macroscale superlubricity. Nat Nanotechnol 2013;8(12):893–4.
[113] Saravanan P, Selyanchyn R, Tanaka H, Darekar D, Staykov A, Fujikawa S, Lyth SM, Sugimura J. Macroscale superlubricity of multilayer polyethylenimine/graphene oxide coatings in different gas environments. ACS Appl Mater Interfaces 2016;8(40):27179–87.
[114] Gong ZB, Jia XL, Ma W, Zhang B, Zhang JY. Hierarchical structure graphitic-like/MoS_2 film as superlubricity material. Appl Surf Sci 2017;413:381–6.
[115] Li JJ, Ge XY, Luo JB. Random occurrence of macroscale superlubricity of graphite enabled by tribo-transfer of multilayer graphene nanoflakes. Carbon 2018;138:154–60.
[116] Berman D, Mutyala KC, Srinivasan S, Sankaranarayanan SKRS, Erdemir A, Shevchenko EV, Sumant AV. Iron-nanoparticle driven tribochemistry leading to superlubric sliding interfaces. Adv Mater Interfaces 2019;6(23):1901416.
[117] Zhang ZY, Du YF, Huang SL, Meng FN, Chen LL, Xie WX, Chang KK, Zhang CH, Lu Y, Lin CT, Li SZ, Parkin IP, Guo DM. Macroscale superlubricity enabled by graphene-coated surfaces. Adv Sci 2020;7(4):1903239.
[118] Androulidakis C, Koukaras EN, Paterakis G, Trakakis G, Galiotis C. Tunable macroscale structural superlubricity in two-layer graphene via strain engineering. Nat Commun 2020;11(1):1595.
[119] Jiang BZ, Zhao ZC, Gong ZB, Wang DL, Yu GM, Zhang JY. Superlubricity of metal-metal interface enabled by graphene and MoWS4 nanosheets. Appl Surf Sci 2020;520:146303.
[120] Huang S, Mutyala KC, Sumant AV, Mochalin VN. Achieving superlubricity with 2D transition metal carbides (MXenes) and MXene/graphene coatings. Mater Today Adv 2021;9:100133.
[121] Li PP, Ji L, Li HX, Chen L, Liu XH, Zhou HD, Chen JM. Role of nanoparticles in achieving macroscale superlubricity of graphene/nano-SiO_2 particle composites. Friction 2022;10(9):1305–16.
[122] Li RY, Yang X, Zhao J, Yue CT, Wang YF, Li JG, Meyer E, Zhang JY, Shi YJ. Operando formation of van der Waals heterostructures for achieving macroscale superlubricity on engineering rough and worn surfaces. Adv Funct Mater 2022;32(18):2111365.
[123] Socoliuc A, Bennewitz R, Gnecco E, Meyer E. Transition from stick-slip to continuous sliding in atomic friction: entering a new regime of ultralow friction. Phys Rev Lett 2004;92(13):134301.
[124] Forcadel N, Imbert C, Monneau R. Homogenization of fully overdamped Frenkel–Kontorova models. J Differ Equ 2009;246(3):1057–97.
[125] Gao EL, Wu BZ, Wang YLY, Jia XZ, Ouyang WG, Liu Z. Computational prediction of superlubric layered heterojunctions. ACS Appl Mater Interfaces 2021;13(28):33600–8.
[126] Engelsberg S, Schrieffer JR. Coupled electron-phonon system. Phys Rev 1963;131(3):993.
[127] Wei ZY, Duan ZQ, Kan YJ, Zhang Y, Chen YF. Phonon energy dissipation in friction between graphene/graphene interface. J Appl Phys 2020;127(1):015105.
[128] Lei Y, Zhang TY, Lin YC, Granzier-Nakajima T, Bepete G, Kowalczyk DA, Lin Z, Zhou D, Schranghamer TF, Dodda A, Sebastian A, Chen YF, Liu YY, Pourtois G, Kempa TJ, Schuler B, Edmonds MT, Quek SY, Wurstbauer U, Wu SM, Glavin NR, Das S, Dash SP, Redwing JM, Robinson JA, Terrones M. Graphene and beyond: recent advances in two-dimensional materials synthesis, properties, and devices. ACS Nanosci Au 2022;2(6):450–85.
[129] Greenwood G, Kim JM, Nahid SM, Lee Y, Hajarian A, Nam S, Espinosa-Marzal RM. Dynamically tuning friction at the graphene interface using the field effect. Nat Commun 2023;14(1):5801.
[130] Woods LM, Mahan GD. Electron-phonon effects in graphene and armchair (10, 10) single-wall carbon nanotubes. Phys Rev B 2000;61(16):10651–63.
[131] Zheng XH, Gao L, Yao QZ, Li QY, Zhang M, Xie XM, Qiao S, Wang G, Ma TB, Di ZF, Luo JB, Wang X. Robust ultra-low-friction state of graphene via moire superlattice confinement. Nat Commun 2016;7:13204.
[132] Smolyanitsky A, Killgore JP, Tewary VK. Effect of elastic deformation on frictional properties of few-layer graphene. Phys Rev B 2012;85(3):035412.
[133] Deng Z, Klimov NN, Solares SD, Li T, Xu H, Cannara RJ. Nanoscale interfacial friction and adhesion on supported versus suspended monolayer and multilayer graphene. Langmuir 2013;29(1):235–43.
[134] Deng Z, Smolyanitsky A, Li QY, Feng XQ, Cannara RJ. Adhesion-dependent negative friction coefficient on chemically modified graphite at the nanoscale. Nat Mater 2012;11(12):1032–7.
[135] Zhao H, Aluru NR. Temperature and strain-rate dependent fracture strength of graphene. J Appl Phys 2010;108(6):064321.
[136] Bylinskii A, Gangloff D, Vuletic V. Tuning friction atom-by-atom in an ion-crystal simulator. Science 2015;348(6239):1115–8.
[137] Bohlein T, Mikhael J, Bechinger C. Observation of kinks and antikinks in colloidal monolayers driven across ordered surfaces. Nat Mater 2012;11(2):126–30.
[138] Hirano M, Shinjo K, Kaneko R, Murata Y. Anisotropy of frictional forces in muscovite mica. Phys Rev Lett 1991;67(19):2642–5.
[139] Ball P. A new twist on superlubricity. Nat Mater 2019;18(8). 774-774.
[140] Feng XF, Kwon S, Park JY, Salmeron M. Superlubric sliding of graphene nanoflakes on graphene. ACS Nano 2013;7(2):1718–24.
[141] Li JJ, Li JF, Luo JB. Superlubricity of graphite sliding against graphene nanoflake under ultrahigh contact pressure. Adv Sci 2018;5(11):1800810.
[142] Li BW, Yin J, Liu XF, Wu HR, Li JD, Li XM, Guo WL. Probing van der Waals interactions at two-dimensional heterointerfaces. Nat Nanotechnol 2019;14(6):567–72.
[143] Tian JS, Yin X, Li JJ, Qi W, Huang P, Chen XC, Luo JB. Tribo-induced interfacial material transfer of an atomic force microscopy probe assisting superlubricity in a WS2/graphene heterojunction. ACS Appl Mater Interfaces 2020;12(3):4031–40.
[144] Kawai S, Benassi A, Gnecco E, Soede H, Pawlak R, Feng XL, Muellen K, Passerone D, Pignedoli CA, Ruffieux P, Fasel R, Meyer E. Superlubricity of graphene nanoribbons on gold surfaces. Science 2016;351(6276):957–61.
[145] Song YM, Gao X, Hinaut A, Scherb S, Huang SY, Glatzel T, Hod O, Urbakh M, Meyer E. Velocity dependence of moire friction. Nano Lett 2022;22(23):9529–36.
[146] Chan N, Balakrishna SG, Klemenz A, Moseler M, Egberts P, Bennewitz R. Contrast in nanoscale friction between rotational domains of graphene on Pt(111). Carbon 2017;113:132–8.
[147] Yin X, Zhang J, Luo T, Cao BQ, Xu JX, Chen XC, Luo JB. Tribochemical mechanism of superlubricity in graphene quantum dots modified DLC films under high contact pressure. Carbon 2021;173:329–38.
[148] Liu YF, Li JJ, Yi S, Ge XY, Chen XC, Luo JB. Enhancement of friction performance of fluorinated graphene and molybdenum disulfide coating by microdimple arrays. Carbon 2020;167:122–31.
[149] Berman D, Narayanan B, Cherukara MJ, Sankaranarayanan SKRS, Erdemir A, Zinovev A, Sumant AV. Operando tribochemical formation of onion-like-carbon leads to macroscale superlubricity. Nat Commun 2018;9:1164.
[150] Li RY, Yang X, Hou DL, Wang YF, Zhang JY. Superlubricity of carbon nanostructural films enhanced by graphene nanoscrolls. Mater Lett 2020;271:127748.
[151] Jin B, Chen GY, He YY, Zhang CH, Luo JB. Lubrication properties of graphene under harsh working conditions. Mater Today Adv 2023;18:100369.
[152] Granick S. Motions and relaxations of confined liquids. Science 1991;253(5026):1374–9.
[153] Granick S, Zhu YX, Lee H. Slippery questions about complex fluids flowing past solids. Nat Mater 2003;2(4):221–7.
[154] Aliyu IK, Mohammed AS, Al-Qutub A. Tribological performance of UHMWPE/GNPs nanocomposite coatings for solid lubrication in bearing application. Tribol Lett 2018;66(4):144.
[155] Nemati N, Emamy M, Yau S, Kim JK, Kim DE. High temperature friction and wear properties of graphene oxide/polytetrafluoroethylene composite coatings deposited on stainless steel. RSC Adv 2016;6(7):5977–87.
[156] Wang L, Tieu AK, Zhu HT, Deng GY, Hai GJ, Wang J, Yang J. The effect of expanded graphite with sodium metasilicate as lubricant at high temperature. Carbon 2020;159:345–56.
[157] Shukla DK, Mukherjee B, Islam A, Keshri AK. Peculiar high temperature tribological behaviour of plasma sprayed graphene nanoplatelets reinforced cerium oxide coatings. Ceram Int 2021;47(12):17809–12.
[158] Xu ZS, Zhang QX, Shi XL, Zhai WZ, Yang K. Tribological properties of TiAl matrix self-lubricating composites containing multilayer graphene and Ti_3SiC_2 at high temperatures. Tribol Trans 2015;58(6):1131–41.
[159] Ibrahim AMM, Shi XL, Zhang A, Yang K, Zhai WZ. Tribological characteristics of NiAl matrix composites with 1.5wt% graphene at elevated temperatures: an experimental and theoretical study. Tribol Trans 2015;58(6):1076–83.
[160] Yang K, Ma HR, Cao ST, Li XX, Li AH, Cao ZZ. Analysis of friction interfaces with sinusoidal microchannels and the hybrid lubrication mechanisms of a tribo-film. Appl Surf Sci 2020;525:146502.

[161] Garcia I, Guerra S, de Damborenea J, Conde A. Reduction of the coefficient of friction of steel-steel tribological contacts by novel graphene-deep eutectic solvents (DESs) lubricants. Lubricants 2019;7(4):37.
[162] Lu GC, Shi XL, Liu XY, Zhou HY, Chen Y, Yang ZY, Huang YC. Tribological performance of functionally gradient structure of graphene nanoplatelets reinforced Ni3Al metal matrix composites prepared by laser melting deposition. Wear 2019;428:417–29.
[163] Wang L, Tieu AK, Hai GJ, Li JQ, Zhu HT, Sang TP, Yang J. Na_2CO_3 and graphene nanocomposites toward efficient lubrication. Carbon 2021;177:138–50.
[164] Wu JY, Liu H, Wang HD, Ma W, Wang TM, Wang QH. Effects of TiO_2 decorated reduced graphene oxide on mechanical and tribological properties of thermosetting polyimide. Compos Interfaces 2022;29(9):985–98.
[165] Arif T, Colas G, Filleter T. Effect of humidity and water intercalation on the tribological behavior of graphene and graphene oxide. ACS Appl Mater Interfaces 2018;10(26):22537–44.
[166] Shi JD, Ma GZ, Han CH, Wang HD, Li GL, Wei AB, Liu YF, Yong QS. The tribological performance in vacuum of DLC coating treated with graphene spraying top layer. Diam Relat Mater 2020;125:108998.
[167] Berman D, Erdemir A, Sumant AV. Reduced wear and friction enabled by graphene layers on sliding steel surfaces in dry nitrogen. Carbon 2013;59:167–75.
[168] Yang YW, Jia WH, Ma LM, Zhu JY, Wang HG, Hou KM, Wang JQ, Yang SR. A feasible construction strategy of GO-based hetero-film with long service life at multi-environments: Effective friction transfer application. Tribol Int 2022;168:107455.
[169] Wang MJ, Liu H, Wang YX, Hou KM, Wang JQ, Yang SR. Stable lubrication in air and vacuum of GO-Al^{3+} coating via strong chemical bonding and reactive sites passivation by aluminum ions. Carbon 2020;160:247–54.
[170] Sun K, Fan X, Yang L, Chen SC, Fan JW, Diao DF. Graphene nanocrystallites induced short run-in period with low electric power at current-carrying sliding interface. Appl Surf Sci 2021;568:150902.
[171] Wang DW, Li FQ, Chen X, Xiang ZY, Zhao F. Probing the effect of the electric current on the tribological performances of the electrical contact surfaces with graphene coating. Tribol Int 2023;178:108121.
[172] Bai T, Liu XL. Effect of magnetic field on the tribological performance of waterborne polyurethane coatings with magnetized graphene oxide. Prog Org Coat 2022;167:106839.
[173] Munoz R, Gómez-Aleixandre C. Review of CVD synthesis of graphene. Chem Vap Depos, 19 (10-12) 2013:297–322.
[174] Li G, Huang SH, Li ZY. Gas-phase dynamics in graphene growth by chemical vapour deposition. Phys Chem Chem Phys 2015;17(35):22832–6.
[175] Bhaviripudi S, Jia XT, Dresselhaus MS, Kong J. Role of kinetic factors in chemical vapor deposition synthesis of uniform large area graphene using copper catalyst. Nano Lett 2010;10(10):4128–33.
[176] Jia KC, Ci HN, Zhang JC, Sun ZT, Ma ZT, Zhu YS, Liu SN, Liu JL, Sun LZ, Liu XT, Sun JY, Yin WJ, Peng HL, Lin L, Liu ZF. Superclean growth of graphene using a cold-wall chemical vapor deposition approach. Angew Chem Int Ed 2020;59(39):17214–8.
[177] Alnuaimi A, Almansouri I, Saadat I, Nayfeh A. Toward fast growth of large area high quality graphene using a cold-wall CVD reactor. RSC Adv 2017;7(82):51951–7.
[178] Shen B, Huang ZW, Ji Z, Lin Q, Chen SL, Cui DJ, Zhang ZN. Bilayer graphene film synthesized by hot filament chemical vapor deposition as a nanoscale solid lubricant. Surf Coat Technol 2019;380:125061.
[179] Anuar NAB, Nor NHM, Awang RB, Nakajima H, Tunmee S, Tripathi M, Dalton A, Goh BT. Low-temperature growth of graphene nanoplatelets by hot-wire chemical vapour deposition. Surf Coat Technol 2021;411:126995.
[180] Boyd DA, Lin WH, Hsu CC, Teague ML, Chen CC, Lo YY, Chan WY, Su WB, Cheng TC, Chang CS, Wu CI, Yeh NC. Single-step deposition of high-mobility graphene at reduced temperatures. Nat Commun 2015;6:6620.
[181] Zafar MA, Jacob MV. Plasma-based synthesis of graphene and applications: a focused review. Rev Mod Plasma Phys 2022;6(1):37.
[182] Li ML, Liu DH, Wei DC, Song XF, Wei DP, Wee ATS. Controllable synthesis of graphene by plasma-enhanced chemical vapor deposition and its related applications. Adv Sci 2016;3(11):1600003.
[183] Shi ZX, Ci HA, Yang XZ, Liu ZF, Sun JY. Direct-chemical vapor deposition-enabled graphene for emerging energy storage: versatility, essentiality, and possibility. ACS Nano 2022;16(8):11646–75.
[184] Bae S, Kim H, Lee Y, Xu XF, Park JS, Zheng Y, Balakrishnan J, Lei T, Kim HR, Song YI, Kim YJ, Kim KS, Özyilmaz B, Ahn JH, Hong BH, Iijima S. Roll-to-roll production of 30-inch graphene films for transparent electrodes. Nat Nanotechnol 2010;5:574–8.
[185] Xu JB, Hu JX, Li Q, Wang RB, Li WW, Guo YF, Zhu YB, Liu FK, Ullah Z, Dong GC, Zeng ZM, Liu LW. Fast batch production of high-quality graphene films in a sealed thermal molecular movement system. Small 2017;13(27):1700651.
[186] Xin H, Li W. A review on high throughput roll-to-roll manufacturing of chemical vapor deposition graphene. Appl Phys Rev 2018;5(3):031105.
[187] Yamada T, Ishihara M, Kim J, Hasegawa M, Iijima S. A roll-to-roll microwave plasma chemical vapor deposition process for the production of 294 mm width graphene films at low temperature. Carbon 2012;50(7):2615–9.
[188] Kobayashi T, Bando M, Kimura N, Shimizu K, Kadono K, Umezu N, Miyahara K, Hayazaki S, Nagai S, Mizuguchi Y, Murakami Y, Hobara D. Production of a 100-m-long high-quality graphene transparent conductive film by roll-to-roll chemical vapor deposition and transfer process. Appl Phys Lett 2013;102(2):023112.
[189] Hesjedal T. Continuous roll-to-roll growth of graphene films by chemical vapor deposition. Appl Phys Lett 2011;98(13):133106.
[190] Polsen ES, McNerny DQ, Viswanath B, Pattinson SW, Hart AJ. High-speed roll-to-roll manufacturing of graphene using a concentric tube CVD reactor. Sci Rep 2015;5:10257.
[191] Sun BJ, Pang JB, Cheng QL, Zhang S, Li YF, Zhang CC, Sun DH, Ibarlucea B, Li Y, Chen D, Fan HM, Han QF, Chao MX, Liu H, Wang JG, Cuniberti G, Han L, Zhou WJ. Synthesis of wafer-scale graphene with chemical vapor deposition for electronic device applications. Adv Mater Technol 2021;6(7):2000744.
[192] Liu FN, Li P, An H, Peng P, McLean B, Ding F. Achievements and challenges of graphene chemical vapor deposition growth. Adv Funct Mater 2022;32(42):2203191.
[193] Weatherup RS, Bayer BC, Blume R, Ducati C, Baehtz C, Schloegl R, Hofmann S. In situ characterization of alloy catalysts for low-temperature graphene growth. Nano Lett 2011;11(10):4154–60.
[194] Li ZC, Wu P, Wang CX, Fan XD, Zhang WH, Zhai XF, Zeng CG, Li ZY, Yang JL, Hou JG. Low-temperature growth of graphene by chemical vapor deposition using solid and liquid carbon sources. ASC Nano 2011;5(4):3385–90.
[195] Zhang B, Lee WH, Piner R, Kholmanov I, Wu YP, Li HF, Ji HX, Ruoff RS. Low-temperature chemical vapor deposition growth of graphene from toluene on electropolished copper foils. ACS Nano 2012;6(3):2471–6.
[196] Davies RH, Dinsdale AT, Gisby JA, Robinson JAJ, Martin SM. MTDATA - thermodynamic and phase equilibrium software from the national physical laboratory. CALPHAD: Comput Coupling Phase Diagr Thermochem 2002;26(2):229–71.
[197] Jang J, Son M, Chung S, Kim K, Cho C, Lee BH, Ham MH. Low-temperature-grown continuous graphene films from benzene by chemical vapor deposition at ambient pressure. Sci Rep 2015;5:17955.
[198] Cushing GW, Johánek V, Navin JK, Harrison I. Graphene growth on Pt(111) by ethylene chemical vapor deposition at surface temperatures near 1000 K. J Phys Chem C 2015;119(9):4759–68.
[199] Shu HB, Tao XM, Ding F. What are the active carbon species during graphene chemical vapor deposition growth? Nanoscale 2015;7(5):1627–34.
[200] Abild-Pedersen F, Greeley J, Studt F, Rossmeisl J, Munter TR, Moses PG, Skulason E, Bligaard T, Norskov JK. Scaling properties of adsorption energies for hydrogen-containing molecules on transition-metal surfaces. Phys Rev Lett 2007;99(1):016105.
[201] Kondrashov II, Rybin MG, Obraztsova EA, Obraztsova ED. Controlled graphene synthesis from solid carbon sources. Phys Status Solidi B 2019;256(9):1800688.
[202] Wu TR, Ding GQ, Shen HL, Wang HM, Sun L, Jiang D, Xie XM, Jiang MH. Triggering the continuous growth of graphene toward millimeter-sized grains. Adv Funct Mater 2013;23(2):198–203.
[203] Lisi N, Buonocore F, Dikonimos T, Leoni E, Faggio G, Messina G, Morandi V, Ortolani L, Capasso A. Rapid and highly efficient growth of graphene on copper by chemical vapor deposition of ethanol. Thin Solid Films 2014;571:139–44.
[204] Kairi MI, Khavarian M, Bakar SAbu, Vigolo B, Mohamed AR. Recent trends in graphene materials synthesized by CVD with various carbon precursors. J Mater Sci 2018;53(2):851–79.
[205] Wassei JK, Mecklenburg M, Torres JA, Fowler JD, Regan BC, Kaner RB, Weiller BH. Chemical vapor deposition of graphene on copper from methane, ethane and propane: evidence for bilayer selectivity. Small 2012;8(9). 1415-142.
[206] Chen JY, Wen YG, Guo YL, Wu B, Huang LP, Xue YZ, Geng DC, Wang D, Yu G, Liu YQ. Oxygen-aided synthesis of polycrystalline graphene on silicon dioxide substrates. J Am Chem Soc 2011;133(44):17548–51.
[207] Song YX, Zhang CR, Li B, Ding GQ, Jiang D, Wang HM, Xie XM. Van der Waals epitaxy and characterization of hexagonal boron nitride nanosheets on graphene. Nanoscale Res Lett 2014;9:367.
[208] Li JZ, Samad A, Schwingenschlögl U, Tian B, Lanza M, Zhang XX. Morphology-control growth of graphene islands by nonlinear carbon supply. Adv Mater 2022;34(44):2206080.
[209] Qin B, Ma HF, Hossain M, Zhong MZ, Xia QL, Li B, Duan XD. Substrates in the synthesis of two-dimensional materials via chemical vapor deposition. Chem Mater 2020;32(24):10321–47.
[210] Liu FN, Li P, An H, Peng P, Mclean B, Ding F. Achievements and challenges of graphene chemical vapor deposition growth. Adv Funct Mater 2022;32(42):2203191.
[211] Xie YD, Cheng T, Liu C, Chen K, Cheng Y, Chen ZL, Qiu L, Cui G, Yu Y, Cui LZ, Zhang MT, Zhang J, Ding F, Liu KH, Liu ZF. Ultrafast catalyst-free graphene growth on glass assisted by local fluorine supply. ACS Nano 2019;13(9):10272–8.
[212] Kim H, Song I, Park C, Son M, Hong M, Kim Y, Kim JS, Shin HJ, Baik J, Choi HC. Copper-vapor-assisted chemical vapor deposition for high-quality and metal-free single-layer graphene on amorphous SiO2 substrate. ACS Nano 2013;7(8):6575–82.
[213] Mishra N, Forti S, Fabbri F, Martini L, McAleese C, Conran B, Whelan PR, Shivayogimath A, Jessen BS, Buss L, Falta J, Aliaj I, Roddaro S, Flege JI, Boggild P, Teo KBK, Coletti C. Wafer-scale synthesis of graphene on sapphire: toward fab-compatible graphene. Small 2020;15(50):1904906.
[214] Xue XD, Wang LP, Yu G. Surface engineering of substrates for chemical vapor deposition growth of graphene and applications in electronic and spintronic devices. Chem Mater 2021;33(23):8960–89.
[215] Li XS, Cai WW, An JH, Kim S, Nah J, Yang DX, Piner R, Velamakanni A, Jung I, Tutuc E, Banerjee SK, Colombo L, Ruoff RS. Large-area synthesis of high-quality and uniform graphene films on copper foils. Science 2009;324(5932):1312–4.
[216] Mattevi C, Kim H, Chhowalla M. A review of chemical vapour deposition of graphene on copper. J Mater Chem 2011;21(10):3324–34.
[217] Lin L, Liu ZF. Graphene synthesis: on-the-spot growth. Nat Mater 2016;15(1):9–10.

[218] Li XS, Cai WW, Colombo L, Ruoff RS. Evolution of graphene growth on Ni and Cu by carbon isotope labeling. Nano Lett 2009;9(12):4268–72.
[219] Kim KS, Lee HJ, Lee CG, Lee SK, Jang H, Ahn JH, Kim JH, Lee HJ. Chemical vapor deposition-grown graphene: the thinnest solid lubricant. ACS Nano 2011;5(6):5107–14.
[220] Chen SS, Cai WW, Piner RD, Suk JW, Wu YP, Ren YJ, Kang JY, Ruoff RS. Synthesis and characterization of large-area graphene and graphite films on commercial Cu-Ni alloy foils. Nano Lett 2011;11(9):3519–25.
[221] Huang M, Biswal M, Park HJ, Jin S, Qu DS, Hong S, Zhu ZL, Qiu L, Luo D, Liu XC, Yang Z, Liu ZL, Huang Y, Lim H, Yoo WJ, Ding F, Wang YL, Lee Z, Ruoff RS. Highly oriented monolayer graphene grown on Cu/Ni(111) alloy foil. ACS Nano 2018;12(6):6117–27.
[222] Liu W, Kraemer S, Sarkar D, Li H, Ajayan PM, Banerjee K. Controllable and rapid synthesis of high-quality and large-area bernal stacked bilayer graphene using chemical vapor deposition. Chem Mater 2014;26(2):907–15.
[223] Vlassiouk IV, Stehle Y, Pudasaini PR, Unocic RR, Rack PD, Baddorf AP, Ivanov IN, Lavrik NV, List F, Gupta N, Bets KV, Yakobson BI, Smirnov SN. Evolutionary selection growth of two-dimensional materials on polycrystalline substrates. Nat Mater 2018;17(4):318–22.
[224] Zou JB, Guan JQ, Wang XY, Du XS. Corrosion and wear resistance improvements in NiCu alloys through flame-grown honeycomb carbon and CVD of graphene coatings. Surf Coat Technol 2023;437:130040.
[225] Fan SY, Chen YN, Xiao S, Shi KJ, Meng XY, Lin SS, Su FH, Su YF, Chu PK. In situ self-adaptive growth of graphene coatings on hard substrates via competitive NiCo catalysis reaction. Carbon 2024;216:118561.
[226] Huang M, Deng BW, Dong F, Zhang LL, Zhang ZY, Chen P. Substrate engineering for CVD growth of single crystal graphene. Small Methods 2021;5(5):2001213.
[227] Wu P, Zhang WH, Li ZY, Yang JL. Mechanisms of graphene growth on metal surfaces: theoretical perspectives. Small 2014;10(11):2136–350.
[228] Edwards RS, Coleman KS. Graphene film growth on polycrystalline metals. Acc Chem Res 2013;46(1):23–30.
[229] Ani MH, Kamarudin MA, Ramlan AH, Ismail E, Sirat MS, Mohamed MA, Azam MA. A critical review on the contributions of chemical and physical factors toward the nucleation and growth of large-area graphene. J Mater Sci 2018;53(10):7095–111.
[230] Zhang JC, Lin L, Jia KC, Sun LZ, Peng HL, Liu ZF. Controlled growth of single-crystal graphene films. Adv Mater 2020;32(1):1903266.
[231] Brune H. Epitaxial growth of thin films. Surf Interface Sci 2014;4:421–77.
[232] Kim H, Saiz E, Chhowalla M, Mattevi C. Modeling of the self-limited growth in catalytic chemical vapor deposition of graphene. N J Phys 2013;15:053012.
[233] Zhang XY, Xu ZW, Hui L, Xin J, Ding F. How the orientation of graphene is determined during chemical vapor deposition growth. J Phys Chem Lett 2012;3(19):2822–7.
[234] Meca E, Lowengrub J, Kim H, Mattevi C, Shenoy VB. Epitaxial graphene growth and shape dynamics on copper: phase-field modeling and experiments. Nano Lett 2013;13(11):5692–7.
[235] Saeed M, Alshammari Y, Majeed SA, Al-Nasrallah E. Chemical vapour deposition of graphene—synthesis, characterization, and applications: a review. Molecules 2020;25(17):3856.
[236] Robertson AW, Warner JH. Hexagonal single crystal domains of few-layer graphene on copper foils. Nano Lett 2011;11(3):1182–9.
[237] Liu W, Li H, Xu C, Khatami Y, Banerjee K. Synthesis of high-quality monolayer and bilayer graphene on copper using chemical vapor deposition. Carbon 2011;49(13):4122–30.
[238] Zhang Y, Zhang LY, Kim P, Ge MY, Li Z, Zhou CW. Vapor trapping growth of single-crystalline graphene flowers: synthesis, morphology, and electronic properties. Nano Lett 2012;12(6):2810–6.
[239] Tripathi K, Gyawali G, Lee SW. CVD-graphene coating for improving friction and wear of grey cast iron at interfaces. ACS Appl Mater Interfaces 2017;9:32336–51.
[240] Losurdo M, Giangregorio MM, Capezzuto P, Bruno G. Graphene CVD growth on copper and nickel: role of hydrogen in kinetics and structure. Phys Chem Chem Phys 2011;13(46):20836–43.
[241] Vlassiouk I, Regmi M, Fulvio PF, Dai S, Datskos P, Eres G, Smirnov S. Role of hydrogen in chemical vapor deposition growth of large single-crystal graphene. ACS Nano 2011;5(7):6069–76.
[242] Zhang XY, Wang L, Xin J, Yakobson BI, Ding F. Role of hydrogen in graphene chemical vapor deposition growth on a copper surface. J Am Chem Soc 2014;136(8):3040–7.
[243] Zhang Y, Li Z, Kim P, Zhang LY, Zhou CW. Anisotropic hydrogen etching of chemical vapor deposited graphene. ASC Nano 2012;6(1):126–32.
[244] Hu JX, Xu JB, Zhao YF, Shi L, Li Q, Liu FK, Ullah Z, Li WW, Guo YF, Liu LW. Roles of oxygen and hydrogen in crystal orientation transition of copper foils for high-quality graphene growth. Sci Rep 2017;7:45358.
[245] Anisur MR, Banerjee PC, Easton CD, Raman RKS. Controlling hydrogen environment and cooling during CVD graphene growth on nickel for improved corrosion resistance. Carbon 2018;127:131–40.
[246] Seah CM, Chai SP, Mohamed AR. Mechanisms of graphene growth by chemical vapour deposition on transition metals. Carbon 2014;70:1–21.
[247] Lee D, Kwon GD, Kim JH, Moyen E, Lee YH, Baik S, Pribat D. Significant enhancement of the electrical transport properties of graphene films by controlling the surface roughness of Cu foils before and during chemical vapor deposition. Nanoscale 2014;6(21):12943–51.
[248] Lu LQ, De Hosson JTM, Pei YT. Low-temperature synthesis of large-area graphene-based carbon films on Ni. Mater Des 2018;144:245–55.
[249] Sun X, Lin L, Sun LZ, Zhang JC, Rui DR, Li JY, Wang MZ, Tan CW, Kang N, Wei D, Xu HQ, Peng HL, Liu ZF. Low-temperature and rapid growth of large single-crystalline graphene with ethane. Small 2018;14(3):1702916.
[250] Singh S, Chen XC, Zhang CH, Gautam RK, Tyagi R, Luo JB. Nickel-catalyzed direct growth of graphene on bearing steel (GCr15) by thermal chemical vapor deposition and its tribological behavior. Appl Surf Sci 2020;502:144135.
[251] Park BJ, Choi JS, Eom JH, Ha H, Kim HY, Lee S, Shin H, Yoon SG. Defect-free graphene synthesized directly at 150 ℃ via chemical vapor deposition with no transfer. ASC Nano 2018;12(2):2008–16.
[252] Nguyen VL, Duong DL, Lee SH, Avila J, Han G, Kim YM, Asensio MC, Jeong SY, Lee YH. Layer-controlled single-crystalline graphene film with stacking order via Cu-Si alloy formation. Nat Nanotechnol 2020;15(10):861–7.
[253] Won MS, Penkov OV, Kim DE. Durability and degradation mechanism of graphene coatings deposited on Cu substrates under dry contact sliding. Carbon 2013;54:472–81.
[254] Patera LL, Africh C, Weatherup RS, Blume R, Bhardwaj S, Castellarin-Cudia C, Knop-Gericke A, Schloegl R, Comelli G, Hofmann S, Cepek C. In situ observations of the atomistic mechanisms of Ni catalyzed low temperature graphene growth. ASC Nano 2013;7(9):7901–12.
[255] Kim H, Mattevi C, Calvo MR, Oberg JC, Artiglia L, Agnoli S, Hirjibehedin CF, Chhowalla M, Saiz E. Activation energy paths for graphene nucleation and growth on Cu. ACS Nano 2012;6(4):3614–23.
[256] Reina A, Jia XT, Ho J, Nezich D, Son HB, Bulovic V, Dresselhaus MS, Kong J. Large area, few-layer graphene films on arbitrary substrates by chemical vapor deposition. Nano Lett 2009;9(1):30–5.
[257] Xu SS, Zhang LP, Wang B, Ruoff RS. Chemical vapor deposition of graphene on thin-metal films. Cell Rep Phys Sci 2021;2(3):100372.
[258] Lee HC, Liu WW, Chai SP, Mohamed AR, Aziz A, Khe CS, Hidayah NMS, Hashim U. Review of the synthesis, transfer, characterization and growth mechanisms of single and multilayer graphene. RSC Adv 2017;7(26):15644–93.
[259] Choi DS, Kin KS, Kim H, Kim TY, Rhy S, Yang CM, Yoon DH, Yang WS. Effect of cooling condition on chemical vapor deposition synthesis of graphene on copper catalyst. ACS Appl Mater Interfaces 2014;6:19574–8.